cause of the aqueous solvent used in the dilution, whereas the osmolarity of TB is higher than that of the control. In contrast, BBG (0.25 mg/mL) has an almost identical osmolarity to the control.

The mean corneal endothelial cell counts were $7728 \pm 268/mm^2$ in the control group, $7642 \pm 317/mm^2$ in the BBG groups, $7501 \pm 230/mm^2$ in the ICG group, and $7030 \pm 246/mm^2$ in the TB group. Thus, although BBG showed marginally less toxicity, there was no significant difference across the 4 groups. In rat's eyes, corneal endothelial cells are known to have a higher proliferative capacity than in human endothelial cells. Our endothelial cell count of rat's eyes is suggestive for clinical use; however, the data do not apply to human endothelial cell counts. Although the corneal endothelial cell count did not change in the observation period in the present study, further research is now needed in human clinical studies.

In conclusion, the results of this study show high biocompatibility of BBG for use in capsular staining. Brilliant blue G demonstrated better-preserved morphologic features of corneal endothelial cells using transmission and scanning electron microscopy than ICG and TB. Also, TUNEL confirmed the lower toxicity of BBG vs TB. Because rat corneal endothelial cells have higher proliferative capacity than human endothelial cells, the rat data do not apply to human eyes, and further detailed studies are needed in human clinical studies. In addition, the BBG solution has an osmolarity similar to that of the physiologic aqueous humor. Thus, BBG is a good alternative dye for capsular staining, with superior staining ability and biocompatibility.

Submitted for Publication: December 23, 2004; final revision received June 22, 2005; accepted June 30, 2005.
Correspondence: Tatsuro Ishibashi, MD, PhD, Department of Ophthalmology, Graduate School of Medical Sciences, Kyushu University, 3-1-1 Maidashi, Higashi-ku, Fukuoka 812-8582, Japan (ishi@eye.med.kyushu-u.ac.jp).
Financial Disclosure: None.
Funding/Support: This study was supported in part by grants-in-aid for scientific research 16791052 and 14571676 from the Japanese Ministry of Education, Science, Sports, and Culture, Tokyo.

REFERENCES

1. Horiguchi M, Miyake K, Ohta I, Ito Y. Staining of the lens capsule for circular continuous capsulorrhexis in eyes with white cataract. *Arch Ophthalmol.* 1998; 116:535-537.
2. Melles GR, de Waard PW, Pameyer JH, Houdijn Beekhuis W. Trypan blue capsule staining to visualize the capsulorhexis in cataract surgery. *J Cataract Refract Surg.* 1999;25:7-9.
3. Dada T, Ray M, Bhartiya P, Vajpayee RB. Trypan-blue–assisted capsulorhexis for trainee phacoemulsification surgeons [letter]. *J Cataract Refract Surg.* 2002; 28:575-576.
4. van Dooren BT, de Waard PW, Poort-van Nouhuys H, Beekhuis WH, Melles GR. Corneal endothelial cell density after trypan blue capsule staining in cataract surgery [letter]. *J Cataract Refract Surg.* 2002;28:574-575.
5. van Dooren BT, Beekhuis WH, Pels E. Biocompatibility of trypan blue with human corneal cells. *Arch Ophthalmol.* 2004;122:736-742.
6. Newsom TH, Oetting TA. Indocyanine green staining in traumatic cataract. *J Cataract Refract Surg.* 2000;26:1691-1693.
7. Kobayashi A, Segawa Y, Nishimura A, Shirao Y, Sugiyama K. Indocyanine green staining for the triple corneal procedure. *Ophthalmic Surg Lasers Imaging.* 2004; 35:23-25.
8. McEnerney JK, Peyman GA. Indocyanine green: a new vital stain for use before penetrating keratoplasty. *Arch Ophthalmol.* 1978;96:1445-1447.
9. Enaida H, Sakamoto T, Hisatomi T, Goto Y, Ishibashi T. Morphological and functional damage of the retina caused by intravitreous indocyanine green in rat eyes. *Graefes Arch Clin Exp Ophthalmol.* 2002;240:209-213.
10. Lee JE, Yoon TJ, Oum BS, Lee JS, Choi HY. Toxicity of indocyanine green injected into the subretinal space: subretinal toxicity of indocyanine green. *Retina.* 2003;23:675-681.
11. Jackson TL, Hillenkamp J, Knight BC, et al. Safety testing of indocyanine green and trypan blue using retinal pigment epithelium and glial cell cultures. *Invest Ophthalmol Vis Sci.* 2004;45:2778-2785.
12. Hisatomi T, Sakamoto T, Murata T, et al. Relocalization of apoptosis-inducing factor in photoreceptor apoptosis induced by retinal detachment in vivo. *Am J Pathol.* 2001;158:1271-1278.
13. Hisatomi T, Sakamoto T, Goto Y, et al. Critical role of photoreceptor apoptosis in functional damage after retinal detachment. *Curr Eye Res.* 2002;24:161-172.
14. Hisatomi T, Sakamoto T, Sonoda KH, et al. Clearance of apoptotic photoreceptors: elimination of apoptotic debris into the subretinal space and macrophage-mediated phagocytosis via phosphatidylserine receptor and integrin alphavbeta3. *Am J Pathol.* 2003;162:1869-1879.
15. Hisatomi T, Enaida H, Sakamoto T, et al. A new method for comprehensive bird's-eye analysis of the surgically excised internal limiting membrane. *Am J Ophthalmol.* 2005;139:1121-1122.
16. Unlu K, Aksunger A, Soker S, Ertem M. Mitomycin C primary trabeculectomy with releasable sutures in primary glaucoma. *Jpn J Ophthalmol.* 2000;44:524-529.
17. Fritz WL. Fluorescein blue, light-assisted capsulorhexis for mature or hypermature cataract. *J Cataract Refract Surg.* 1998;24:19-20.
18. Pandey SK, Werner L, Escobar-Gomez M, Roig-Melo EA, Apple DJ. Dye-enhanced cataract surgery, part 1: anterior capsule staining for capsulorhexis in advanced/white cataract. *J Cataract Refract Surg.* 2000;26:1052-1059.
19. Hoffer KJ, McFarland JE. Intracameral subcapsular fluorescein staining for improved visualization during capsulorhexis in mature cataracts [letter]. *J Cataract Refract Surg.* 1993;19:566.
20. Gale JS, Proulx AA, Gonder JR, Mao AJ, Hutnik CM. Comparison of the in vitro toxicity of indocyanine green to that of trypan blue in human retinal pigment epithelium cell cultures. *Am J Ophthalmol.* 2004;138:64-69.
21. Sippy BD, Engelbrecht NE, Hubbard GB, et al. Indocyanine green effect on cultured human retinal pigment epithelial cells: implication for macular hole surgery. *Am J Ophthalmol.* 2001;132:433-435.
22. Engelbrecht NE, Freeman J, Sternberg P Jr, et al. Retinal pigment epithelial changes after macular hole surgery with indocyanine green–assisted internal limiting membrane peeling. *Am J Ophthalmol.* 2002;133:89-94.
23. Kawaji T, Hirata A, Inomata Y, Koga T, Tanihara H. Morphological damage in rabbit retina caused by subretinal injection of indocyanine green. *Graefes Arch Clin Exp Ophthalmol.* 2004;242:158-164.
24. Iriyama A, Uchida S, Yanagi Y, et al. Effects of indocyanine green on retinal ganglion cells. *Invest Ophthalmol Vis Sci.* 2004;45:943-947.
25. Haritoglou C, Gandorfer A, Gass CA, Schaumberger M, Ulbig MW, Kampik A. Indocyanine green–assisted peeling of the internal limiting membrane in macular hole surgery affects visual outcome: a clinicopathologic correlation. *Am J Ophthalmol.* 2002;134:836-841.
26. Gass CA, Haritoglou C, Schaumberger M, Kampik A. Functional outcome of macular hole surgery with and without indocyanine green–assisted peeling of the internal limiting membrane. *Graefes Arch Clin Exp Ophthalmol.* 2003;241:716-720.
27. Sharma N, Bhartiya P, Sinha R, Vajpayee RB. Trypan blue assisted phacoemulsification by residents in training [letter]. *Clin Experiment Ophthalmol.* 2002; 30:386-387.
28. Sperling S. Evaluation of the endothelium of human donor corneas by induced dilation of intercellular spaces and trypan blue. *Graefes Arch Clin Exp Ophthalmol.* 1986;224:428-434.
29. Jacob S, Agarwal A, Agarwal S, Chowdhary S, Chowdhary R, Bagmar AA. Trypan blue as an adjunct for safe phacoemulsification in eyes with white cataract. *J Cataract Refract Surg.* 2002;28:1819-1825.
30. Rezai KA, Farrokh-Siar L, Gasyna EM, Ernest JT. Trypan blue induces apoptosis in human retinal pigment epithelial cells. *Am J Ophthalmol.* 2004;138:492-495.
31. Holley GP, Alam A, Kiri A, Edelhauser HF. Effect of indocyanine green intraocular stain on human and rabbit corneal endothelial structure and viability: an in vitro study. *J Cataract Refract Surg.* 2002;28:1027-1033.
32. Stalmans P, Van Aken EH, Veckeneer M, Feron EJ, Stalmans I. Toxic effect of indocyanine green on retinal pigment epithelium related to osmotic effects of the solvent. *Am J Ophthalmol.* 2002;134:282-285.

Cellular Migration Associated With Macular Hole

A New Method for Comprehensive Bird's-Eye Analysis of the Internal Limiting Membrane

Toshio Hisatomi, MD, PhD; Hiroshi Enaida, MD, PhD; Taiji Sakamoto, MD, PhD; Takaaki Kanemaru, MD; Tadahisa Kagimoto, MD; Ichiro Yamanaka, MD, PhD; Akifumi Ueno, MD; Takao Nakamura, MD, PhD; Yasuaki Hata, MD, PhD; Tatsuro Ishibashi, MD, PhD

Objective: To elucidate the pathogenesis of macular hole formation, focusing in particular on the possible role of cellular migration on the cortical vitreous and internal limiting membrane (ILM) around the macular hole.

Methods: To gain a comprehensive overview of the ILM excised in macular hole surgery (n=36), the ILMs were carefully unfolded and spread out onto glass slides as continuous flat sheets that each contained a macular hole. The specimens were observed by light microscopy and transmission electron microscopy (n=9), and the cellular distribution was analyzed by scanning electron microscopy in a quantitative manner (n=27). Immunohistochemistry for glial fibrillary acidic protein and cytokeratin 18 was carried out for cellular characterization. Cellular proliferation was assessed by immunohistochemistry for proliferating cell nuclear antigen and Ki-67.

Results: Cellular migration was not apparent around the macular hole in the early stage of development of the macular hole (stage 2, 0 μm). As the macular hole passed through the later stages of development, cellular migration developed around the macular hole (stage 3, 84 μm) and the area of cellular migration gradually enlarged (stage 4, 420 μm). The immunophenotypic analysis showed that these cells were mainly glial fibrillary acidic protein–positive glial cells and cytokeratin 18–positive retinal pigment epithelial cells. The proliferating cell nuclear antigen and Ki-67 immunohistochemistry showed that some of these cells were proliferating on the ILM.

Conclusions: Cellular migration on the ILM is not necessary for the initial formation of a macular break. Cellular migration developed after the macular break occurred, and the migration and proliferation increased gradually from the macular hole.

Clinical Relevance: This study provides a new method for understanding the ultrastructural analysis of the pathogenesis of the macular hole.

Arch Ophthalmol. 2006;124:1005-1011

THE PATHOGENESIS OF THE IDiopathic macular hole is still not fully understood; however, there is agreement on the important role of vitreous attachment and vitreous traction to the underlying internal limiting membrane (ILM) and the retina in the developmental process of the macular hole. Avila et al[1] and Kakehashi et al[2] proposed that anteroposterior traction in the vitreous can cause a macular break. It was suggested that contraction of the prefoveal vitreous cortex might cause tangential traction leading to a macular tear.[3-6] It was also suggested that the premacular vitreous cortex is the posterior wall of the vitreous pocket and that anterior traction by premacular vitreous cortex would lead to intraretinal cyst formation at the fovea following macular hole formation.[7-9] In recent years, ultrasonography,[10,11] confocal laser tomography,[12-14] and optical coherence tomography[15-21] have provided high-resolution cross-sectional images of the retina and vitreous in vivo. Gass[3,5] proposed a classification for the development of a macular hole according to 4 stages. Stage 1 is characterized by focal retinal detachment, stage 2 by early hole formation, stage 3 by a fully developed macular hole without posterior vitreous detachment (PVD), and stage 4 by a macular hole with PVD.

Cellular migration is hypothesized to be one of the major causes of contraction of extracellular matrix such as vitreous cortex.[22-24] Some biomicroscopical studies and histological examinations of surgical and postmortem specimens have identified premacular tissue that may cause tangential traction to the retina.[22,25-27] In addition, histological examinations of excised ILMs demonstrated that migrating cells of various origins were located on the ILM and that these cells were associated with collagen fi-

Author Affiliations:
Department of Ophthalmology (Drs Hisatomi, Enaida, Kagimoto, Yamanaka, Ueno, Nakamura, Hata, and Ishibashi) and Morphology Core (Dr Kanemaru), Graduate School of Medical Sciences, Kyushu University, Fukuoka, and Department of Ophthalmology, Kagoshima University School of Medicine, Kagoshima (Dr Sakamoto), Japan.

Table. Summary of the 27 Excised Internal Limiting Membranes Analyzed by Scanning Electron Microscopy From Various Stages of Development of the Macular Hole*

Specimen No.	Macular Hole Stage	Fixation	Immunohistochemistry†	Hematoxylin-Eosin Staining†	Distance of Cellular Migration From Macular Hole, μm
1	2	PFA	...	‡	0
2	2	GA	...	...	0
3	2	GA	...	...	0
4	2	GA	...	...	0
5	2	PFA	GFAP, CK18	...	0
6	3	GA	...	...	0
7	3	GA	...	...	NA
8	3	GA	...	...	0
9	3	GA	...	...	0
10	3	GA	...	...	0
11	3	GA	...	...	0
12	3	PFA	...	...	NA
13	3	PFA	GFAP, CK18	...	224
14	3	GA	...	...	0
15	3	PFA	GFAP, CK18	...	451
16	4	GA	...	...	359
17	4	GA	...	...	NA
18	4	GA	...	...	0
19	4	GA	...	...	93
20	4	PFA	...	...	NA
21	4	PFA	...	‡	810
22	4	GA	...	...	0
23	4	PFA	Ki-67	...	1210
24	4	PFA	GFAP, CK18	...	850
25	4	PFA	Ki-67	...	320
26	4	PFA	PCNA	...	390
27	4	PFA	PCNA	...	138

Abbreviations: CK18, cytokeratin 18; GA, glutaraldehyde; GFAP, glial fibrillary acidic protein; NA, not applicable; PCNA, proliferating cell nuclear antigen; PFA, paraformaldehyde.

*Twenty-seven specimens were confirmed as stage 2 in 5 eyes, stage 3 in 10 eyes, and stage 4 in 12 eyes. Successful expansion of the folded internal limiting membrane was obtained in 23 specimens, and immunohistochemistry and hematoxylin-eosin staining were carried out in 8 and 2 specimens, respectively.

†Ellipses indicate that the specimens were not analyzed by the method.

‡Specimen was analyzed by hematoxylin-eosin staining.

bers of various diameters.[26-28] Other histological studies[22,25,29] examining postmortem eyes with macular holes noted a high incidence of epiretinal formation in the macular area of the eyes. However, their detailed pathogenesis, especially the role and involvement of cellular migration on the ILM, still remains unclear.

We propose a new method for a topographic bird's-eye analysis of the whole excised ILM. In this study, we describe detailed structures of the ILM around the idiopathic macular hole, the complex association of migrating and proliferating cells, and the extracellular matrix conferred by the developing stages of the macular hole. We examine the characterization and the proliferation of the distributing cells around the macular hole on the ILM.

METHODS

ILM PEELING PROCEDURE

Thirty-nine eyes of 38 patients who were diagnosed as having various stages of the idiopathic macular hole were prospectively studied clinically from January 2002 to July 2004. Biomicroscopical analysis of both the macular and vitreomacular relationships was carried out to identify the macular hole, and each was then graded according to the classification developed by Gass.[3,5,30] A high-resolution optical coherence tomographic examination was used to confirm the state of PVD in each case. The stages of development of the macular holes were confirmed as stage 2 in 8 eyes, stage 3 in 13 eyes, and stage 4 in 15 eyes (total, 36 eyes). All of the data accumulation was carried out with approval from the ethics committee of Kyushu University, Fukuoka, Japan, and was performed in accordance with ethical standards in the 1989 Declaration of Helsinki. After informed consent was obtained from each patient, the patients underwent a standard 3-port pars plana vitrectomy. Balanced salt solution (BSS Plus; Alcon Laboratories, Fort Worth, Tex) was used as an irrigation solution. Triamcinolone acetonide (Kenakolt-A; Bristol Pharmaceuticals KK, Tokyo, Japan), a water-insoluble white corticosteroid, was used for visualizing the vitreous hyaloid as previously described[31-34] (in a 1.0-mL triamcinolone acetonide suspension). If necessary, posterior hyaloid detachment was induced by suction or forceps around the optic nerve head. The vitreous was removed and PVD was extended to the periphery. The ILM was then peeled off with ILM forceps intended to be 3 disc diameters surrounding the macular hole, and fluid-gas exchange was performed through an extrusion cannula over the optic nerve head and macular hole. Twenty-percent sulfahexafluoride gas was then injected after closure of the scleral incisions. Postoperatively, patients were asked to keep a face-down position for at least 5 days.

TRANSMISSION ELECTRON MICROSCOPY OF THE EXCISED ILM

To carry out transmission electron microscopy, the 12 excised specimens (stage 2 in 4 eyes, stage 3 in 4 eyes, and stage 4 in 4 eyes) were immediately placed in 4% glutaraldehyde for fixation. Of the 12 specimens, 9 of them (stage 2 in 3 eyes, stage 3 in 3 eyes, and stage 4 in 3 eyes) were then postfixed in 2% veronal acetate buffer osmium tetroxide, dehydrated in ethanol and water, and embedded in Epon.[35] Ultrathin sections were cut from blocks and mounted on copper grids. The specimens were observed with a JEM 100CX electron microscope (JEOL, Tokyo). Three specimens were further examined by flat-preparation transmission electron microscopy.

FLAT-PREPARATION TRANSMISSION ELECTRON MICROSCOPY

Three fixed specimens (stage 2 in 1 eye, stage 3 in 1 eye, and stage 4 in 1 eye) were dehydrated in ethanol and water, extracted as flat sheets with fine needles under a biomicroscope equipped with dark-field illumination (Nikon, Tokyo), and placed onto a glass slide. Then, the expanded ILMs were embedded in Epon. Ultrathin sections were cut from blocks and mounted on copper grids. The specimens were observed with a JEM 100CX electron microscope.

FLAT PREPARATION FOR COMPREHENSIVE BIRD'S-EYE ANALYSIS OF THE ILM

For scanning electron microscopy, 27 specimens were processed. Fifteen of the excised specimens were fixed in 4% glutaraldehyde. Twelve of the specimens were fixed in 4% paraformaldehyde for light microscopy and immunohistochemistry and then were analyzed by scanning electron microscopy. The fixed ILM was extracted as a flat sheet with fine needles under a biomicroscope equipped with dark-field illumination (Nikon) and placed onto a glass slide. When at least one fourth of the complete macular hole was clearly recognized on the expanded ILM (n=23; 4 specimens were excluded from the total of 27 specimens; **Table**), immunochemistry, scanning electron microscopy, and cellular distribution studies were carried out. Two specimens were stained by hematoxylin-eosin and observed by light microscopy.

IMMUNOHISTOCHEMISTRY OF THE EXPANDED ILM

The ILMs were fixed in 4% paraformaldehyde in phosphate-buffered saline, extracted as whole sheets, and placed onto a glass slide (n=8). The specimens were air dried. The first antibodies against glial fibrillary acidic protein (Dako, Tokyo) (n=4), cytokeratin 18 (Chemicon, Temecula, Calif) (n=4), proliferating cell nuclear antigen (PCNA) (Chemicon) (n=2), and Ki-67 (Dako) (n=2) were used for 2 hours at room temperature. The second antibodies labeled with Cy5 (Zymed Laboratories, San Francisco, Calif) and rhodamine (Cappel, Aurora, Ohio) were used for 1 hour at room temperature. The specimens were also stained with 4′,6-diamino-2-phenylindole dihydrochloride for nuclear staining and observed with a fluorescence microscope (Table). The immunohistochemical control experiments included a negative control and an isotype control using the specific IgG subtype. All of the specimens for immunohistochemistry were dehydrated in ethanol and water and then analyzed by scanning electron microscopy.

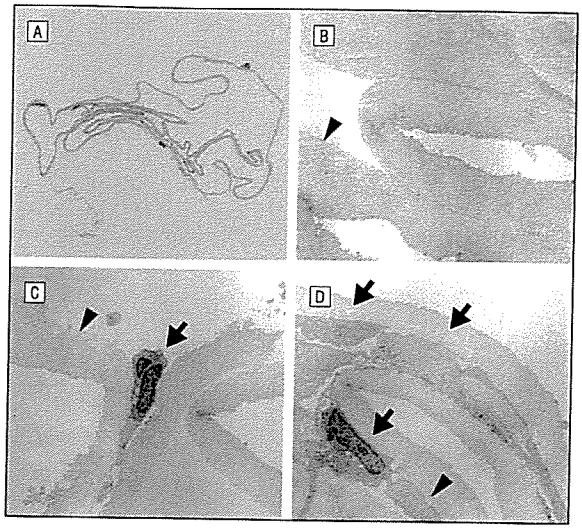

Figure 1. Vertical analysis of the excised internal limiting membrane (ILM). A, Light micrograph of a semithin section of the ILM stained by Azur II, showing characteristic sinusoidal folding (original magnification ×100). B, Transmission electron microscopy showed collagen membranous tissue with a smooth inner (vitreous) surface and an irregular outer (retinal) surface. In the early stage of the macular hole (stage 2), cells were rarely seen. The extracellular matrix, namely, posterior vitreous hyaloid, was seen on the excised ILM intermingled with the distributed cells (arrowhead) (original magnification ×2000). C, Some migrating cells (arrow) were seen on the inner surface of the ILM in stage 3 of development of the macular hole. Again, the extracellular matrix, namely, posterior vitreous hyaloid, was seen on the excised ILM intermingled with the distributed cells (arrowhead) (original magnification ×2000). D, In the later stage (stage 4), significant cellular migration (arrows) was observed on the ILM. The extracellular matrix, namely, posterior vitreous hyaloid, was seen on the excised ILM intermingled with the distributed cells (arrowhead) (original magnification ×2000).

SCANNING ELECTRON MICROSCOPY

The expanded ILMs were dehydrated in ethanol and water on a glass slide. The specimens were saturated in t-butyl alcohol, and critical-point drying (Eiko, Tokyo) was performed. The glass slide was cut into a 10-mm square. The specimens were then placed on stubs by means of self-adhering carbon tabs and sputtered with gold of 20-nm thickness by an argon plasma coater (Eiko).[36,37] The specimens were observed with a JSM 840 electron microscope (JEOL).

CELLULAR DISTRIBUTION ON THE ILM

Cellular distribution was observed in 23 specimens (stage 2 in 5 eyes, stage 3 in 8 eyes, and stage 4 in 10 eyes) (Table) by scanning electron microscopy, and the results were analyzed according to the macular hole staging proposed by Gass.[3,5,30] The distance from the top of the cellular distribution to the edge of the macular hole on the ILM was measured and analyzed using analysis software (MacScope; Mitani, Fukui, Japan). The results were expressed as means±SDs. The *t* test was used to calculate the probability by comparing data between the groups, and $P<.05$ was considered to be statistically significant.

RESULTS

VERTICAL ANALYSIS OF PEELED ILM

Light microscopical examination of semithin sections showed characteristic sinusoidal folds of complexly folded ILM (**Figure 1**A). Transmission electron microscopy

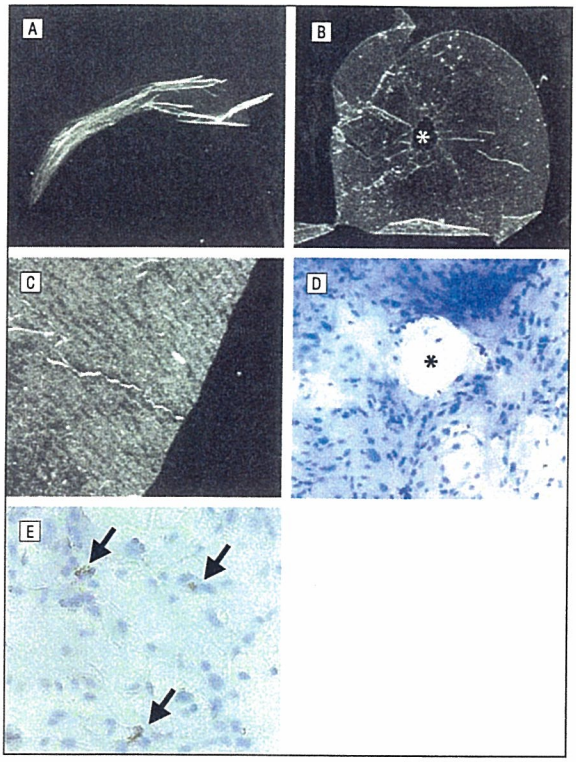

Figure 2. Topographic bird's-eye analysis of the internal limiting membrane (ILM) by light microscopy and fluorescence microscopy. The complexly folded excised ILM (A) extended onto a glass slide showed the intact ILM sheet containing an ILM defect corresponding to the area of the macular hole (asterisk) (B) (original magnification ×4). C, A dark-field illumination image showed that the ILM has the characteristic multilinear pattern associated with the underlying nerve fibers of the ganglion cells (original magnification ×10). D, The hematoxylin-eosin–stained section showed migrating cells around the macular hole (asterisk) (original magnification ×200). E, Some of the cells on the ILM were pigmented cells (arrows) (original magnification ×400).

showed collagen membranous tissue with a smooth inner (vitreous) surface and an irregular outer (retinal) surface (Figure 1B). In the early stage of the macular hole (stage 2), cellular migration was rarely seen (Figure 1B). Some cells, namely, glial cells, retinal pigment epithelial cells, and origin-unknown fibroblast-like cells, were seen on the inner surface of the ILM in the middle stages (stage 3) (Figure 1C) of the macular hole and were seen often in the later stages (stage 4) (Figure 1D). Some cellular membranes and organelles derived from underlying Muller cells were occasionally seen on the outer surface of the ILM; however, there were no changes according to the stage of development of the macular holes (Figure 1B-D). We could not identify the location of the macular hole in complexly folded ILM by ultrathin cross sections.

HORIZONTAL ANALYSIS OF EXPANDED ILM

Light microscopical examination of the excised whole ILM (**Figure 2**A) spread out onto a glass slide showed the intact ILM sheet containing a macular hole (Figure 2B). Dark-field illumination micrography showed that the ILM had the characteristic multilinear pattern associated with the underlying nerve fibers of the ganglion cells (Figure 2C). The hematoxylin-eosin–stained section showed migrating cells around the macular hole (stage 4) (Figure 2D). A few pigmented cells were seen among the distributing cells around the macular hole on the ILM (Figure 2E).

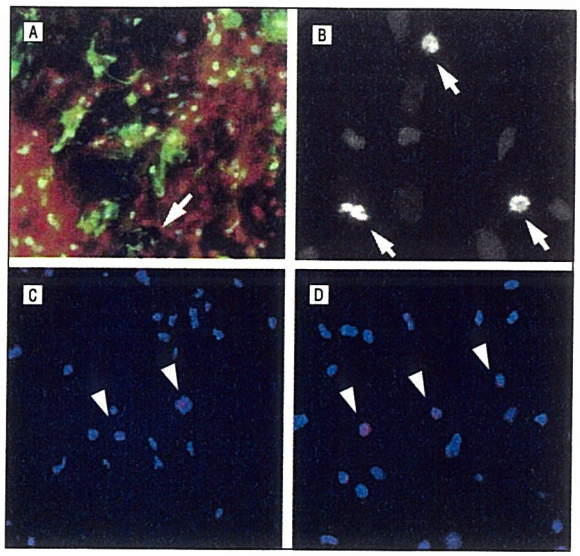

Figure 3. Immunohistochemical analysis of the distributed cells on the internal limiting membrane. A, Double immunohistochemistry of glial fibrillary acidic protein (green) and cytokeratin 18 (red) showed a mosaic-like migration pattern of glial fibrillary acidic protein–positive glial cells and cytokeratin 18–positive retinal pigment epithelial cells. Some of the cytokeratin 18–positive cells were pigmented (arrow) (original magnification ×200). B, Nuclear staining by 4′,6-diamino-2-phenylindole dihydrochloride showed chromosomes of dividing nuclei (arrows) (original magnification ×1000). Immunohistochemistry of proliferating cell nuclear antigen (C) and Ki-67 (D) showed proliferating cells (arrowheads) among the distributed cells on the internal limiting membrane (original magnification ×400).

IMMUNOHISTOCHEMICAL ANALYSIS

Immunohistochemical analysis revealed that most of the dispersed cells on the ILM were glial fibrillary acidic protein–positive glial cells (**Figure 3**A). There were also cytokeratin 18–positive retinal pigment epithelial cells among the glial cells (Figure 3A). These cells formed a continuous cellular sheet around the macular hole on the ILM. To investigate whether these cells were migrating and/or proliferating on the ILM, we examined their proliferation by 2 different proliferating cell markers, PCNA and Ki-67. Proliferating cell nuclear antigen is a 36-kd proliferation-associated antigen, and Ki-67 is a large nuclear antigen preferentially expressed during all of the active phases of the cell cycle but absent in resting cells. Nuclear staining by 4′,6-diamino-2-phenylindole dihydrochloride showed chromosomes of dividing nuclei (Figure 3B). Both PCNA and Ki-67 showed positive staining in the nucleus of the proliferating cells (Figure 3C and D). The PCNA-positive cells and Ki-67–positive cells accounted for 7% and 9%, respectively, of the total cells on the ILM. The proliferating cells dispersed around the distributed cells around the macular hole, and an obvious proliferating front was not observed in the specimens.

VERTICAL ANALYSIS OF EXPANDED ILM

Light microscopical examination of semithin sections of the expanded ILM showed a linear shape of the ILM

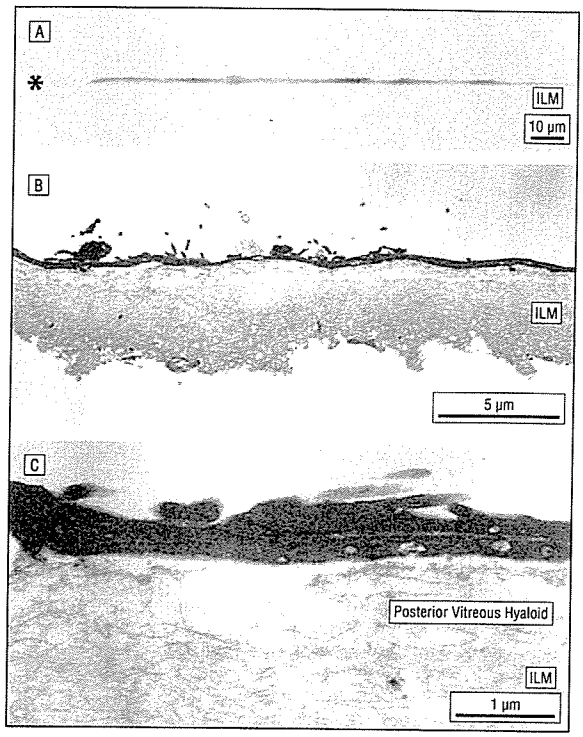

Figure 4. Vertical observation of the expanded internal limiting membrane (ILM). A, Light microscopical examination of a semithin section of the expanded ILM showed the linear shape of the ILM. On the expanded ILM, few Azur II–stained cells were seen around the ILM defect corresponding to the area of the stage 4 macular hole (asterisk) (original magnification ×600). Transmission electron microscopy showed the expanded linear ILM and migrating cells (original magnification ×2000) (B) as well as dense collagen fibers, namely, residual posterior vitreous hyaloid between the ILM and migrating cells (original magnification ×6600) (C).

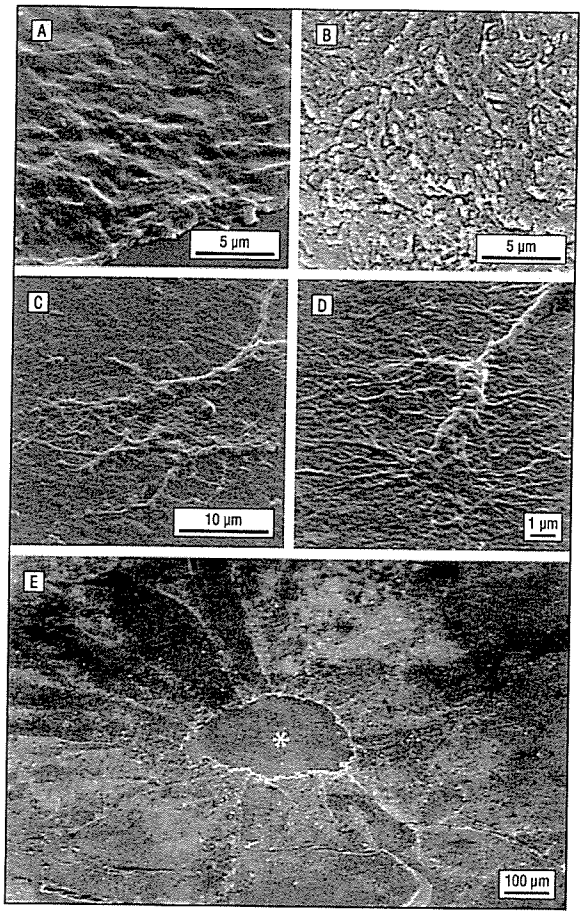

Figure 5. Topographic analysis of the internal limiting membrane (ILM) by scanning electron microscopy. Scanning electron microscopy revealed a smooth inner surface of the excised ILM, where migrating cells from the macular hole were rarely seen in the early stage (stage 2) of development of the macular hole (A), and revealed a rough outer surface of the excised ILM (B) (original magnification ×3000). Migrating cells from the macular hole were more prominent in the later stage (stage 4) of development of the macular hole (original magnification ×1800) (C), showing flat and sticking morphological features and spreading filopodia on the ILM (original magnification ×8000) (D). E, A topographic bird's-eye view of the expanded ILM showed no cellular migration around the ILM defect corresponding to the area of the stage 2 macular hole (asterisk) (original magnification ×75).

(**Figure 4**A). On the expanded ILM, few Azur II–stained cells were shown around the ILM defect corresponding to the area of the macular hole at stage 4, providing better spatial understanding of the ILM. Transmission electron microscopy demonstrated the expanded linear ILM and migrating cells (Figure 4B) as well as dense collagen fibers, namely, residual posterior hyaloid between the ILM and migrating cells (Figure 4C).

SCANNING ELECTRON MICROSCOPY

Scanning electron microscopy revealed a smooth inner surface (**Figure 5**A) and rough outer surface (Figure 5B) of the ILM. This dense collagen layer is a basement membrane of Muller cells, namely, the ILM, and demonstrates the characteristic smooth surface. Neither fibrous collagen nor fibrillar vitreous collagen are smooth surfaced by scanning electron microscopy. In the early stages of development of the macular hole, migrating cells were not apparent on the inner surface of the ILM around the macular hole (Figure 5A). Notably, in the later stages, migrating cells were clearly visible around the ILM defect corresponding to the area of the macular hole (Figure 5C), indicating that these cells were migrating away from the macular hole. Cellular migration occurred on the ILM, showing flat and sticking morphological features and spreading filopodia on the ILM (Figure 5D). A topographic image of the expanded ILM showed no cellular migration around the ILM defect corresponding to the area of the macular hole at stage 2 (Figure 5E).

CELLULAR MIGRATION FROM THE MACULAR HOLE

The distance of cellular migration from the ILM defect corresponding to the area of the macular hole gradually increased through each stage of development of the macular hole (**Figure 6**). The cellular migration occurred from the edge of the macular hole and developed to the peripheral area of the ILM (Figure 6A-C). In most cases, cellular migration was observed as a continuous sheet of cells around the macular hole (Figure 6B and C).

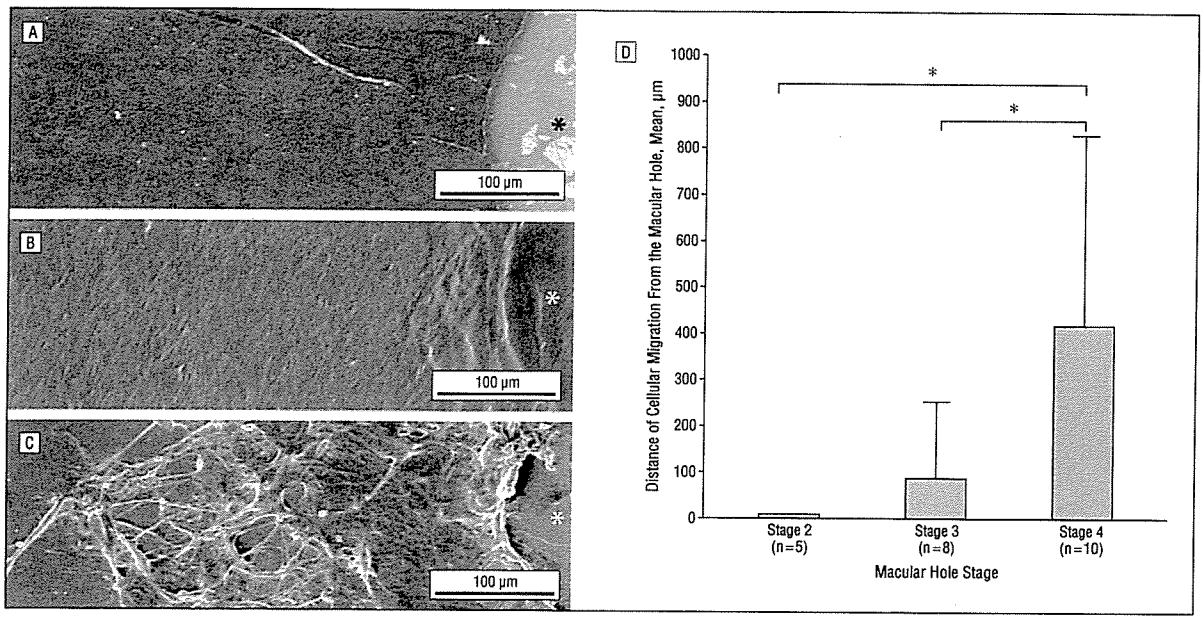

Figure 6. Quantitative analysis of cellular migration from the macular hole. The representative developmental stages of cellular migration on the internal limiting membrane from the internal limiting membrane defect corresponding to the area of the macular hole (asterisks) are shown for stage 2 (A), stage 3 (B), and stage 4 (C) (original magnification ×140). D, The distance of cellular migration from the edge of the macular hole was measured and analyzed using analysis software (MacScope; Mitani, Fukui, Japan). The *t* test was used to calculate the probability by comparing data between the groups, and $P<.05$ was considered to be statistically significant (asterisks). The area of cellular migration gradually enlarged as the macular hole passed through the later stages of development. Error bars indicate SDs.

COMMENT

This study demonstrates that cellular migration around the macular hole develops after the macular break occurs and that cellular migration occurs from the macular hole and enlarges on the ILM. To our knowledge, this is the first article clearly showing that cellular migration on the ILM is not necessary for the initial formation of a macular break.

COMPREHENSIVE TOPOGRAPHIC ANALYSIS OF EXCISED ILM

Some previous histological studies[26-28] demonstrated cellular migration on the ILM around the macular hole; however, this was based on findings from the ultrathin partial cross sections of the ILM, leaving the origin and distribution of the cells largely unknown, as shown in Figure 1. We propose a topographic analysis of the whole excised ILM that enables understanding of cellular migration, especially its origin, frequency, distribution, and relationship with the macular hole (Figure 6). Whereas a cross section gives a snapshot of a limited area of excised complexly folded ILM at a particular time point (Figure 1), horizontal observation enables a comprehensive analysis of spatial distribution that offers a temporal perspective of cellular migration around a macular hole in its process of development (Figure 6).

DISTRIBUTED CELLS AROUND THE MACULAR HOLE

The ultrastructural studies[23,27,28,38] of migrating cells and epiretinal membranes have found them to be glial cells, retinal pigment epithelium, myofibroblasts, and so on. Our light microscopical studies demonstrate that some of the migrating cells were pigmented cells (Figure 2E), and immunohistochemical studies also demonstrate a mosaic-like migration pattern of glial fibrillary acidic protein–positive glial cells and cytokeratin 18–positive retinal pigment epithelial cells (Figure 3A). These cells were intermingled to form an epiretinal membrane as a continuous cellular sheet on the ILM (Figure 2E, Figure 3A, Figure 4B, and Figure 5C). To further estimate the cellular proliferation on the ILM, we examined their proliferation by 2 different proliferating cell markers, PCNA and Ki-67. Although the proliferating cells dispersed around the distributed cells around the macular hole, an obvious proliferating front was not observed in the specimens.

ROLE OF CELLULAR MIGRATION IN THE PATHOGENESIS OF THE MACULAR HOLE

Figure 6A shows a complete lack of cellular migration in the early stage (stage 2) of development of the macular hole. In contrast, Figure 6B shows cellular development around the edge of the macular hole, and Figure 6C shows a large amount of cellular migration from the macular hole to the peripheral area. Notably, in the later stage of development of the macular hole, some specimens showed no cellular migration around the macular hole (Table). Our results confirm that the initial break of the macular hole is not dependent on cellular migration around the macular hole (Figure 6D). In contrast, cellular migration developed after the macular break and expanded from the edge of the macular hole to the periphery (Figure 4A and Figure 6A-C), finally forming an

epiretinal membrane on the ILM. This cellular migration and its contraction of the extracellular matrix on the ILM (Figure 1B-D and Figure 4) might lead to further progression of the macular hole (stage 3) and might keep the macular hole open even after PVD (stage 4).

The role of cellular migration in the pathogenesis of the macular hole remains quite unclear. We provide a comprehensive bird's-eye analysis of the ultrastructure of the ILM and demonstrate cellular migration and proliferation in a quantitative manner, proposing the association of cellular migration to the pathogenesis of a macular hole.

Submitted for Publication: September 8, 2004; final revision received April 14, 2005; accepted April 19, 2005.
Correspondence: Toshio Hisatomi, MD, PhD, Department of Ophthalmology, Graduate School of Medical Sciences, Kyushu University, 3-1-1 Maidashi, Higashi-ku, Fukuoka 812-8582, Japan (hisatomi@med.kyushu-u.ac.jp).
Financial Disclosure: None reported.
Funding/Support: This work was supported in part by grants-in-aid for scientific research 16791052 from the Japanese Ministry of Education, Science, Sports, and Culture, Tokyo.
Acknowledgment: We thank Eve Sockett for editing the manuscript.

REFERENCES

1. Avila MP, Jalkh AE, Murakami K, Trempe CL, Schepens CL. Biomicroscopic study of the vitreous in macular breaks. *Ophthalmology.* 1983;90:1277-1283.
2. Kakehashi A, Schepens CL, Trempe CL. Vitreomacular observations, I: vitreomacular adhesion and hole in the premacular hyaloid. *Ophthalmology.* 1994; 101:1515-1521.
3. Gass JD. Idiopathic senile macular hole: its early stages and pathogenesis. *Arch Ophthalmol.* 1988;106:629-639.
4. Johnson RN, Gass JD. Idiopathic macular holes: observations, stages of formation, and implications for surgical intervention. *Ophthalmology.* 1988;95:917-924.
5. Gass JD. Reappraisal of biomicroscopic classification of stages of development of a macular hole. *Am J Ophthalmol.* 1995;119:752-759.
6. Gass JD. Muller cell cone, an overlooked part of the anatomy of the fovea centralis: hypotheses concerning its role in the pathogenesis of macular hole and foveomacular retinoschisis. *Arch Ophthalmol.* 1999;117:821-823.
7. Kishi S, Shimizu K. Posterior precortical vitreous pocket. *Arch Ophthalmol.* 1990; 108:979-982.
8. Kishi S, Hagimura N, Shimizu K. The role of the premacular liquefied pocket and premacular vitreous cortex in idiopathic macular hole development. *Am J Ophthalmol.* 1996;122:622-628.
9. Kishi S, Takahashi H. Three-dimensional observations of developing macular holes. *Am J Ophthalmol.* 2000;130:65-75.
10. Dugel PU, Smiddy WE, Byrne SF, Hughes JR, Gass JD. Macular hole syndromes: echographic findings with clinical correlation. *Ophthalmology.* 1994; 101:815-821.
11. Johnson MW, Van Newkirk MR, Meyer KA. Perifoveal vitreous detachment is the primary pathogenic event in idiopathic macular hole formation. *Arch Ophthalmol.* 2001;119:215-222.
12. Bartsch DU, Intaglietta M, Bille JF, Dreher AW, Gharib M, Freeman WR. Confocal laser tomographic analysis of the retina in eyes with macular hole formation and other focal macular diseases. *Am J Ophthalmol.* 1989;108:277-287.
13. Weinberger D, Stiebel H, Gaton DD, Priel E, Yassur Y. Three-dimensional measurements of idiopathic macular holes using a scanning laser tomograph. *Ophthalmology.* 1995;102:1445-1449.
14. Beausencourt E, Elsner AE, Hartnett ME, Trempe CL. Quantitative analysis of macular holes with scanning laser tomography. *Ophthalmology.* 1997;104:2018-2029.
15. Puliafito CA, Hee MR, Lin CP, et al. Imaging of macular diseases with optical coherence tomography. *Ophthalmology.* 1995;102:217-229.
16. Gaudric A, Haouchine B, Massin P, Paques M, Blain P, Erginay A. Macular hole formation: new data provided by optical coherence tomography. *Arch Ophthalmol.* 1999;117:744-751.
17. Takahashi H, Kishi S, Ebato K, Hagimura N, Shimizu K, Kamei Y. Tomographic features of a lamellar macular hole formation and a lamellar hole that progressed to a full-thickness macular hole. *Am J Ophthalmol.* 2000;130:677-679.
18. Spaide RF, Wong D, Fisher Y, Goldbaum M. Correlation of vitreous attachment and foveal deformation in early macular hole states. *Am J Ophthalmol.* 2002; 133:226-229.
19. Uemoto R, Yamamoto S, Aoki T, Tsukahara I, Yamamoto T, Takeuchi S. Macular configuration determined by optical coherence tomography after idiopathic macular hole surgery with or without internal limiting membrane peeling. *Br J Ophthalmol.* 2002;86:1240-1242.
20. Sato H, Kawasaki R, Yamashita H. Observation of idiopathic full-thickness macular hole closure in early postoperative period as evaluated by optical coherence tomography. *Am J Ophthalmol.* 2003;136:185-187.
21. Drexler W, Sattmann H, Hermann B, et al. Enhanced visualization of macular pathology with the use of ultrahigh-resolution optical coherence tomography. *Arch Ophthalmol.* 2003;121:695-706.
22. Guyer DR, Green WR, de Bustros S, Fine SL. Histopathologic features of idiopathic macular holes and cysts. *Ophthalmology.* 1990;97:1045-1051.
23. Yooh HS, Brooks HL Jr, Capone A Jr, L'Hernault NL, Grossniklaus HE. Ultrastructural features of tissue removed during idiopathic macular hole surgery. *Am J Ophthalmol.* 1996;122:67-75.
24. Hirayama K, Hata Y, Noda Y, et al. The involvement of the rho-kinase pathway and its regulation in cytokine-induced collagen gel contraction by hyalocytes. *Invest Ophthalmol Vis Sci.* 2004;45:3896-3903.
25. Frangieh GT, Green WR, Engel HM. A histopathologic study of macular cysts and holes. *Retina.* 1981;1:311-336.
26. Smiddy WE, Michels RG, de Bustros S, de la Cruz Z, Green WR. Histopathology of tissue removed during vitrectomy for impending idiopathic macular holes. *Am J Ophthalmol.* 1989;108:360-364.
27. Messmer EM, Heidenkummer HP, Kampik A. Ultrastructure of epiretinal membranes associated with macular holes. *Graefes Arch Clin Exp Ophthalmol.* 1998; 236:248-254.
28. Kampik A, Green WR, Michels RG, Nase PK. Ultrastructural features of progressive idiopathic epiretinal membrane removed by vitreous surgery. *Am J Ophthalmol.* 1980;90:797-809.
29. Rosa RH Jr, Glaser BM, de la Cruz Z, Green WR. Clinicopathologic correlation of an untreated macular hole and a macular hole treated by vitrectomy, transforming growth factor-beta 2, and gas tamponade. *Am J Ophthalmol.* 1996;122: 853-863.
30. Gass JD. Idiopathic senile macular hole: its early stages and pathogenesis. 1988. *Retina.* 2003;23:629-639.
31. Enaida H, Hata Y, Ueno A, et al. Possible benefits of triamcinolone-assisted pars plana vitrectomy for retinal diseases. *Retina.* 2003;23:764-770.
32. Sakamoto T, Miyazaki M, Hisatomi T, et al. Triamcinolone-assisted pars plana vitrectomy improves the surgical procedures and decreases the postoperative blood-ocular barrier breakdown. *Graefes Arch Clin Exp Ophthalmol.* 2002;240:423-429.
33. Matsumoto H, Enaida H, Hisatomi T, et al. Retinal detachment in morning glory syndrome treated by triamcinolone acetonide-assisted pars plana vitrectomy. *Retina.* 2003;23:569-572.
34. Sonoda KH, Sakamoto T, Enaida H, et al. Residual vitreous cortex after surgical posterior vitreous separation visualized by intravitreous triamcinolone acetonide. *Ophthalmology.* 2004;111:226-230.
35. Hisatomi T, Sakamoto T, Murata T, et al. Relocalization of apoptosis-inducing factor in photoreceptor apoptosis induced by retinal detachment in vivo. *Am J Pathol.* 2001;158:1271-1278.
36. Hisatomi T, Sakamoto T, Sonoda KH, et al. Clearance of apoptotic photoreceptors: elimination of apoptotic debris into the subretinal space and macrophage-mediated phagocytosis via phosphatidylserine receptor and integrin alphavbeta3. *Am J Pathol.* 2003;162:1869-1879.
37. Nakamura T, Murata T, Hisatomi T, et al. Ultrastructure of the vitreoretinal interface following the removal of the internal limiting membrane using indocyanine green. *Curr Eye Res.* 2003;27:395-399.
38. Campochiaro PA, Van Niel E, Vinores SA. Immunocytochemical labeling of cells in cortical vitreous from patients with premacular hole lesions. *Arch Ophthalmol.* 1992;110:371-377.

PRECLINICAL INVESTIGATION OF INTERNAL LIMITING MEMBRANE STAINING AND PEELING USING INTRAVITREAL BRILLIANT BLUE G

HIROSHI ENAIDA, MD,* TOSHIO HISATOMI, MD,*
YOSHINOBU GOTO, MD,† YASUAKI HATA, MD,* AKIFUMI UENO, MD,*
MUNEKI MIURA, MD,* TOSHIAKI KUBOTA, MD,‡
TATSURO ISHIBASHI, MD*

Purpose: To investigate the effects of intravitreal brilliant blue G (BBG) on the morphology and functions of the retina and its possible use for staining and peeling of the internal limiting membrane (ILM).

Methods: Rat eyes (n = 78) underwent gas compression vitrectomy. BBG solution was then injected into the vitreous cavity. The eyes were enucleated at 2 weeks and 2 months. Light as well as electron microscopy, terminal nick-end labeling staining, and electroretinography (ERG) were used to investigate retinal damage and function. To test the clinical potential of BBG, ILM staining was evaluated in primate eyes after pars plana vitrectomy followed by ILM peeling.

Results: In the rat eyes, no pathologic changes were observed with light microscopy. Electron microscopy revealed that high doses of BBG induced vacuolization in the inner retinal cells, but apoptosis was not detected. There was no reduction in the amplitude of the ERG waves. In the primate eyes, the ILM was clearly visualized after the intravitreous injection of BBG and was peeled off easily from the retina.

Conclusions: These results demonstrate that BBG, which has low potential for toxicity, high staining ability, and ease of handling, is a good candidate dye for ILM peeling.

RETINA 26:623–630, 2006

The internal limiting membrane (ILM) is the innermost layer of the retina. It forms a boundary between the vitreous and the retina. The ILM acts as a structural support for the Müller cells of the retina. Alterations in the structure of the retina due to cellular proliferation may cause distortion of the ILM, leading to the formation of epiretinal membranes (ERMs) and macular holes. Removal of the ILM can successfully alleviate these vitreoretinal diseases; however, difficulties in visualization of the virtually translucent ILM can present technical challenges in this procedure. It is now widely recognized that without surgical adjuvant it is extremely difficult to remove the membranes due to the poor visibility of the ILM and ERMs. Staining of the ILM is therefore one of the most important developments in surgery for such vitreoretinal diseas-

From the *Department of Ophthalmology and the †Department of Clinical Neurophysiology, Graduate School of Medical Sciences, Kyushu University, Fukuoka, Japan; and the ‡Department of Ophthalmology, University of Occupational and Environmental Health, Kitakyushu, Japan.

Supported in part by Grant-in-Aids 16791052 and 14571676 for Scientific Research from the Japanese Ministry of Education, Science, Sports and Culture.

Reprint requests: Tatsuro Ishibashi, MD, Department of Ophthalmology, Graduate School of Medical Sciences, Kyushu University, 3-1-1 Maidashi, Higashi-ku, Fukuoka, 812-8582, Japan; e-mail: ishi@eye.med.kyushu-u.ac.jp

es.[1–4] Development of indocyanine green (ICG) staining and trypan blue (TB) staining has greatly facilitated peeling of ILM and ERMs in the treatment of various vitreoretinal diseases, and as a result, these staining procedures are now widely used by many surgeons.[5–7] However, numerous clinical and experimental reports have recently suggested that intravitreal injections of ICG and TB can cause retinal damage.[8–21]

In a previous study, we screened various dyes, focusing on their safety and ability to stain membranes. The results of our screening demonstrated that brilliant blue G (BBG) capsular staining contributed to better visualization during continuous curvilinear capsulorhexis in pig eyes than the other dyes tested.[22] Furthermore, the standard staining dose of the dye resulted in no apparent complications and produced minimal changes on the corneal endothelium in rat eyes.[22] Because BBG has an excellent safety record from its use in corneal endothelium and capsular staining, we selected BBG as a potential dye for ILM peeling.

In the present study, we examined the effects of intravitreal BBG on the retina using morphologic and functional analyses in rat models. We also investigated the ability of BBG to stain the ILM of primate eyes.

Materials and Methods

All procedures conformed to the Association for Research in Vision and Ophthalmology Statement for the Use of Animals in Ophthalmic and Vision Research and the guidelines for animal care produced by Kyushu University (Fukuoka, Japan).

Surgical Procedure for Intravitreal BBG in Rat Eyes

Brown Norway rats (78 males; age, 8 weeks; Kyudo, Fukuoka, Japan) were anesthetized with an intraperitoneal injection of ketamine hydrochloride at a dose of 75 mg/kg body weight. One eye from each animal (total of 6 per dose group) was vitrectomized using 0.05 mL of pure SF_6 gas as described previously.[8,23–27] After gas injection, 0.05 mL of BBG solution was injected into the vitreous cavity of each vitrectomized eye using a microscope for enhanced magnification during surgery. The BBG solution (Coomassie BBG 250; Sigma–Aldrich, St. Louis, MO) was prepared at concentrations of 0.01 mg/mL, 0.1 mg/mL, 1.0 mg/mL, and 10 mg/mL using dilution in intraocular irrigating solution (OPEGUARD-MA; Senjyu Pharmaceutical, Osaka, Japan) and sterilized through a 0.22-μm syringe filter. The mean osmolarity was determined using an osmotic pressure meter (OSMO STATION; Arkray, Kyoto, Japan), and the pH of each solution was determined for all concentrations prepared (Table 1). The final concentration was determined according to the ICG solution used in vitrectomies for humans (2.5–5.0 mg/mL),[8] to provide the rats with a safe dose of BBG that would also produce good staining. Twenty-four sham-operated eyes (injected with SF_6 followed by 0.05 mL of intraocular irrigating solution) were used as controls.

Table 1. Characterization of BBG Solution

Solution	Osmolarity (mosm/KgH_2O)	pH
Control*	298	7.33
BBG, 10 mg/mL	310	7.41
BBG, 1.0 mg/mL	300	7.42
BBG, 0.1 mg/mL	298	7.41
BBG, 0.01 mg/mL	298	7.41
Saline	285	7.40
BSS plus†	305	7.10

*OPEGUARD-MA (Senjyu Pharmaceutical, Osaka, Japan).
†Santen, Osaka, Japan.
BBG, brilliant blue G; BSS, balanced salt solution.

Light Microscopy

The eyes were enucleated and fixed in 10% paraformaldehyde on day 14 (n = 30; 6 per dose and control group) and at 2 months (n = 30; 6 per dose and control group) after surgery. Whole eyes were cut approximately along the vertical meridian. Paraffin-embedded sections were stained with hematoxylin–eosin, and each section was examined using light microscopy.

Transmission Electron Microscopy

The eyes were enucleated on day 14 and at 2 months after surgery and fixed in 1% glutaraldehyde and 1% paraformaldehyde in phosphate-buffered saline. The specimens were postfixed in veronal acetate buffer osmium tetroxide (2%), dehydrated in ethanol and water, and embedded in Epon (Epon 812 Resin, CHIYODA JYUNYAKU INC., Tokyo, Japan). Ultrathin sections were cut from blocks and mounted on copper grids. The specimens were observed with a JEM 100CX electron microscope (JEOL, Tokyo, Japan).[28]

TdT-dUTP Terminal Nick-End Labeling (TUNEL)

Apoptotic cell death was detected using TdT-dUTP TUNEL as described previously.[29] A cryostat was used to produce 4-μm sections from samples fixed in 4% paraformaldehyde and embedded in paraffin. TUNEL staining was performed with the ApopTag

Fluorescein Direct In Situ Apoptosis Detection Kit (Intergen, New York) according to the manufacturer's protocol. The sections were costained with propidium iodide (Molecular Probes, Eugene, OR), thus allowing observation of the cell nuclei by a fluorescence microscope (Olympus, Tokyo, Japan). Ten sections from each eye specimen were selected at random and observed using the microscope.

Electroretinography (ERG)

After gas injection, 0.05 mL of BBG solution (1 mg/mL and 10 mg/mL) or intraocular irrigating solution was injected into the vitreous cavity. There were six rats in each dose group and six controls. At time points of 14 days and 2 months, the rats were kept in a dark room for one night, with only dim red illumination, and anesthetized with an intraperitoneal injection of 15 μL/g of body weight of saline solution containing ketamine (1 mg/mL), xylazine (0.4 mg/mL), and urethane (40 mg/mL). ERG was then performed as previously described.[8,27,30,31] The pupils were dilated with 2.5% phenylephrine hydrochloride and 1% tropicamide drops and showed maximal dilatation before ERG recording. The cornea was anesthetized with 1% proparacaine hydrochloride drops, and the rats were then placed on a heating pad throughout the experiment. A wire electrode, coated with 1% methylcellulose, was placed over the cornea for ERG recording. A similar wire electrode placed in the mouth served as a reference electrode, while a needle electrode inserted into the tail was grounded. The responses were differentially amplified (0.8–1,200 Hz), averaged, and stored using a computer. White (xenon) strobe flashes were presented in a Ganzfeld stimulator (VPA-10; Cadwell, Kennewick, WA) against an achromatic adapting field. Dark-adapted (rod-mediated) ERG was performed first to check the response stability at both intensities. Each rat was then adapted to dark background luminance for 20 minutes, a period sufficient to achieve a stable level of response. Thereafter, dark-adapted *a* (rod-mediated) ERG and dark-adapted *b* (bipolar and Müller cell–mediated) ERG were performed at a flash luminance of 1.30 log cd s/m^2. The responses to five successive flashes at an interstimulus interval of 1 minute were then averaged to determine the dark-adapted responses. The rats were then exposed to a white light–adapting field (1.50 log cd/m^2) for at least 25 minutes, and then light-adapted *b* (cone-mediated) ERG was performed at a flash luminance of 1.30 log cd s/m^2 (rod-desensitized condition in rats). The responses to 50 successive flashes made at 2 Hz were averaged. The results of the ERG amplitudes were evaluated using the Student's *t*-test, and $P < 0.05$ was considered statistically significant.

ILM Staining by BBG in Primate Eyes

Because ILM peeling is impossible in rat eyes, we examined the ability of BBG to stain the ILM in primate eyes. Two eyes from two cynomolgus monkeys 3 years of age were used in this study. The animals were restrained in a squeeze cage and injected intramuscularly in the thigh with 20 mg/kg ketamine hydrochloride (Sankyo Yell Pharmaceutical Products, Japan) for general anesthesia. The monkeys were subsequently transported to an operating department. Surgery consisted of standard three-port pars plana vitrectomy with induction of a posterior vitreous detachment by suction with a vitrectomy cutter using triamcinolone acetonide injection for vitreous visualization.[32–35]

Ten milligrams of BBG was dissolved in 20 mL of intraocular irrigating solution and sterilized with a syringe filter. The final concentration of BBG was 0.5 mg/mL. The prepared BBG solution (0.5 mL) was then injected gently into the vitreous cavity and washed out immediately with balanced salt solution (BSS plus; Santen, Osaka, Japan). Removal of the ILM was performed using ILM forceps. The instruments were then removed, and the sclerotomy ports were closed using 7-0 polygalactin sutures. Postoperative examinations included slit-lamp microscopy and ophthalmoscopy on days 1, 3, and 14. Fluorescein angiography was performed on day 14.

Results

Characterization of the BBG Solution

BBG is also known as acid blue 90 and Coomassie BBG. Aside from our previous publication, to our knowledge, there are no reported studies investigating the toxicity of BBG for ophthalmic use.[22] Table 1 shows the osmolarity and pH of the BBG solution at different concentrations. The osmolarity and pH of BBG were found to be similar to those of intraocular irrigating solutions.

Effect of Intravitreal BBG on the Retina

Light Microscopy

After intravitreal injection of BBG, no toxic effects of BBG, such as corneal edema, severe retinal edema, or endophthalmitis, were observed by surgical microscopy over a period of 2 months. The eyes were enucleated on day 14 and at 2 months after surgery. The normal structure of the retina was preserved in the

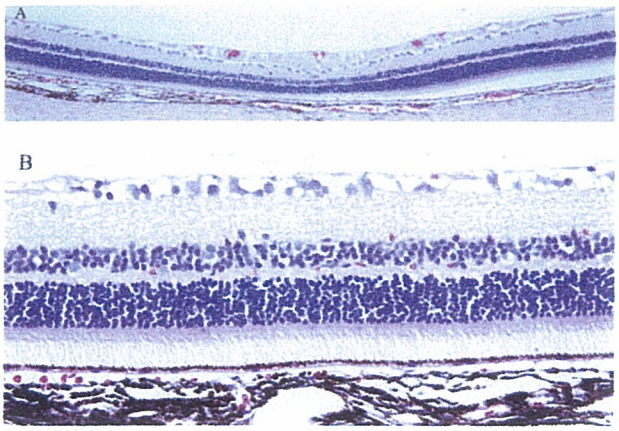

Fig. 1. Light microscopic photography of rat eyes injected with intravitreal brilliant blue G (10 mg/mL; 0.05 mL per eye) visualized at 14 days. No significant change in the retinal construction was observed (original magnification: **A,** ×200; **B,** ×400).

eyes injected with the highest doses of BBG (10 mg/mL) both on day 14 and at 2 months. In addition, no infiltration of inflammatory cells was observed (Fig. 1; day 14). The normal structure of retina was also retained in the groups injected with lower doses of BBG, and no sign of cellular degeneration was observed in the sections on day 14 or at 2 months.

Transmission Electron Microscopy

Some specimens injected with the highest dose of BBG (10 mg/mL) showed vacuolization in the ganglion cells and Müller cell processes of nerve fibers both on day 14 (Fig. 2A; day 14) and at 2 months. Although the same changes were also found in the group injected with 1 mg/mL BBG, the grade of vacuolization was less than in the 10 mg/mL group (Fig. 2B). Vacuolization was not observed in the groups receiving lower doses or in the controls. Among all groups, no remarkable changes were observed in the retina, including the inner nuclear, outer nuclear, and retinal pigment epithelial cell layers.

Apoptotic Cell Death Detected by TUNEL

Because there have been several recent reports regarding damage of the retinal cells by ICG and TB dependent on apoptosis,[16–21] we investigated apoptotic cell death by TUNEL. In the group administered the highest doses of BBG (10 mg/mL), 1 case of apoptotic cell death was observed from among 10 sections. However, the apoptotic cell ratio was not significantly different from that observed in control sections (Fig. 3; day 14). In groups injected with lower doses of BBG, no TUNEL staining was observed in the retina on day 14. Furthermore, retinal cells in all BBG dose groups had not undergone apoptotic cell death after 2 months.

ERG

To evaluate the retinal function after BBG injection, we also performed ERG in the high-dose groups (1.0 mg/mL and 10 mg/mL). The absence of cataracts was confirmed in all rats before measurements were taken. Figure 4A represents the dark-adapted and light-adapted ERG waveforms of the responses of the control and high-dose groups on day 14. The ampli-

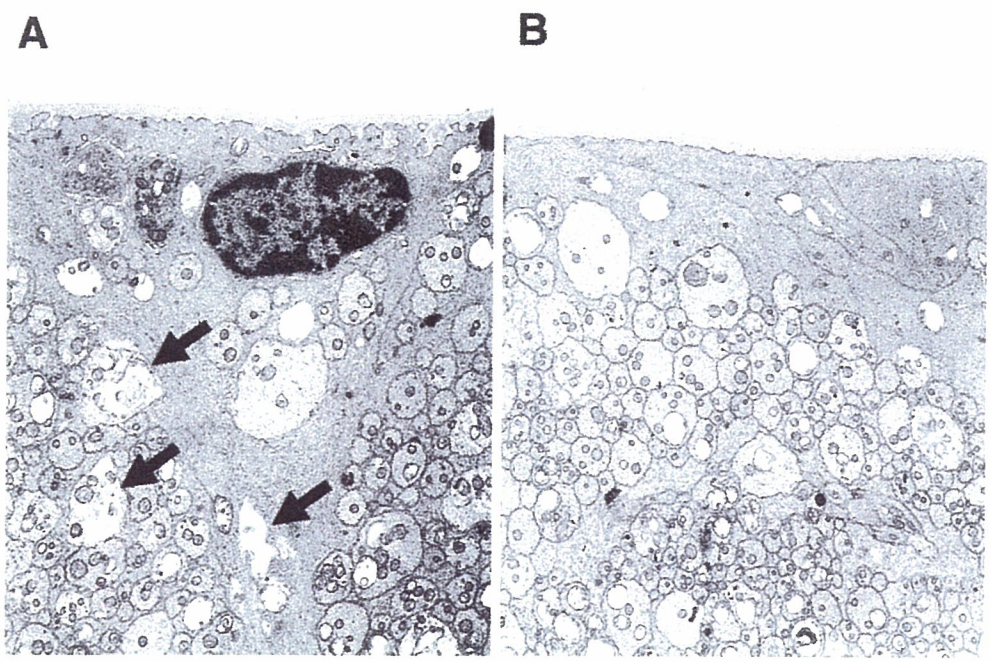

Fig. 2. Transmission electron microscopic photography of the rat eyes injected with intravitreal brilliant blue G (10 mg/mL and 1 mg/mL; 0.05 mL per eye) visualized at 14 days. In the highest dose group (10 mg/mL), arrows show vacuolization in the ganglion cells and Müller cell processes of some specimens at day 14 (**A**). Although the same changes were also found in the 1 mg/mL group (**B**), the grade of vacuolization was less than in the 10 mg/mL group (original magnification, ×2,000).

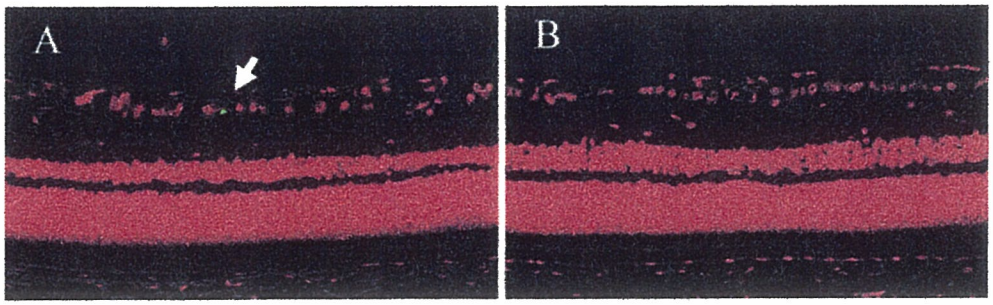

Fig. 3. Apoptotic cell death detected by terminal nick-end labeling. In the highest dose (10 mg/mL) group, 1 case of apoptotic cell death was observed in 10 sections (**A**; day 14); however, the apoptotic cell ratio was not significantly higher than that of the control specimens (**B**; day 14) (original magnification, ×400).

tudes of dark-adapted responses obtained at the beginning of the experiments showed a low variability between groups. Although a slight reduction in the mean maximal amplitude of the dark-adapted *a* waves (Fig. 4B; day 14) on day 14 was observed in a dose-dependent manner in the high-dose groups, there was no significant difference in the maximal wave amplitude compared with the controls (10 mg/mL, $P = 0.054$; and 1.0 mg/mL, $P = 0.063$; *t* test). In addition, dark-adapted *b* waves (10 mg/mL, $P = 0.553$; and 1.0

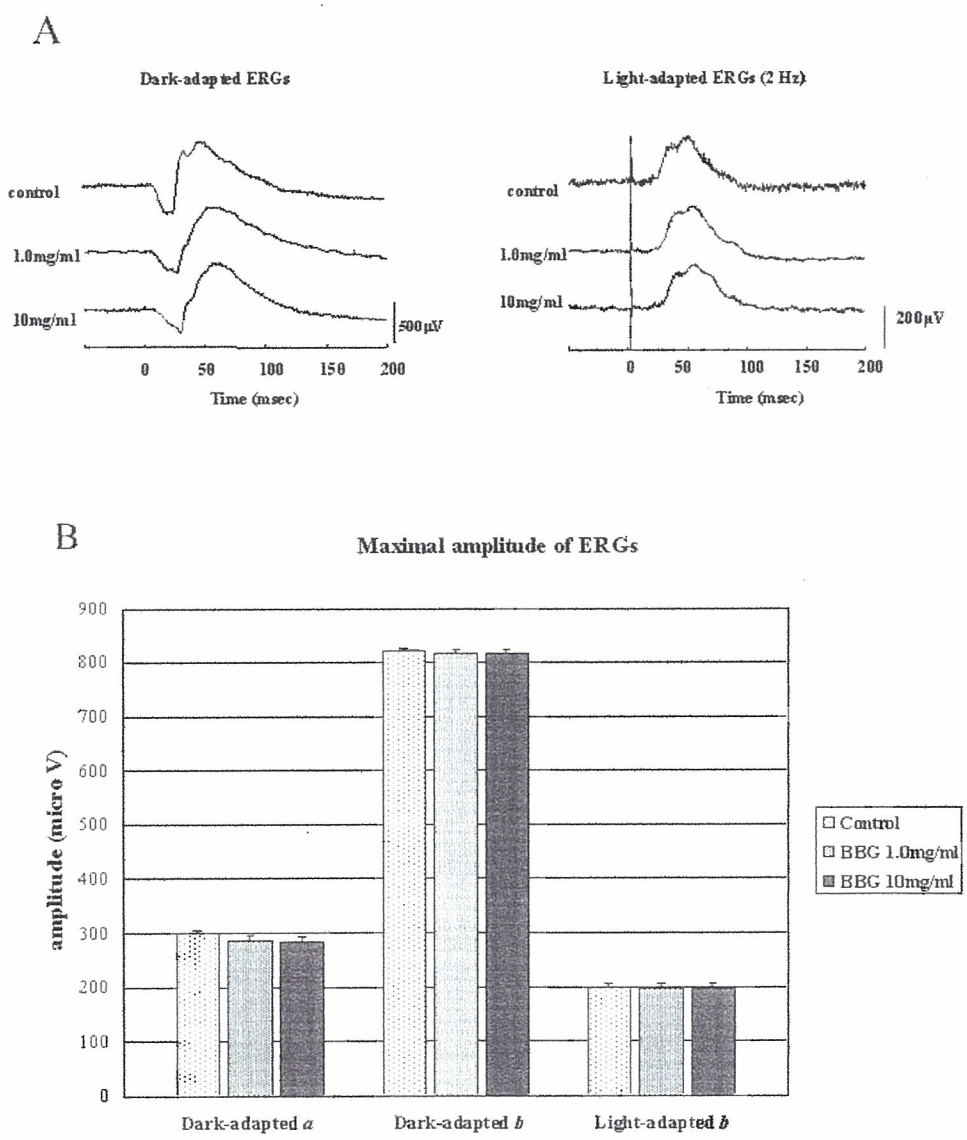

Fig. 4. Waveforms and maximal amplitude of electroretinograms (ERGs) in rat eyes. **A,** ERG traces showing the dark-adapted responses (**left**) and the light-adapted responses (**right**) of the control and intravitreal high-dose brilliant blue G (BBG) injection groups at 14 days after injection. All waves were clearly recorded. Although a slight reduction in the mean maximal amplitude of the dark-adapted *a* waves was observed in a dose-dependent manner on day 14, there was no significant difference when compared with the control group (10 mg/mL, $P = 0.054$; and 1.0 mg/mL, $P = 0.063$; *t* test). Dark-adapted *b* waves and light-adapted *b* wave ERGs demonstrated no remarkable reduction. There was no statistically significant difference between the amplitudes (**B**; day 14). Data are expressed as mean ± SEM of the amplitude as compared with the control group.

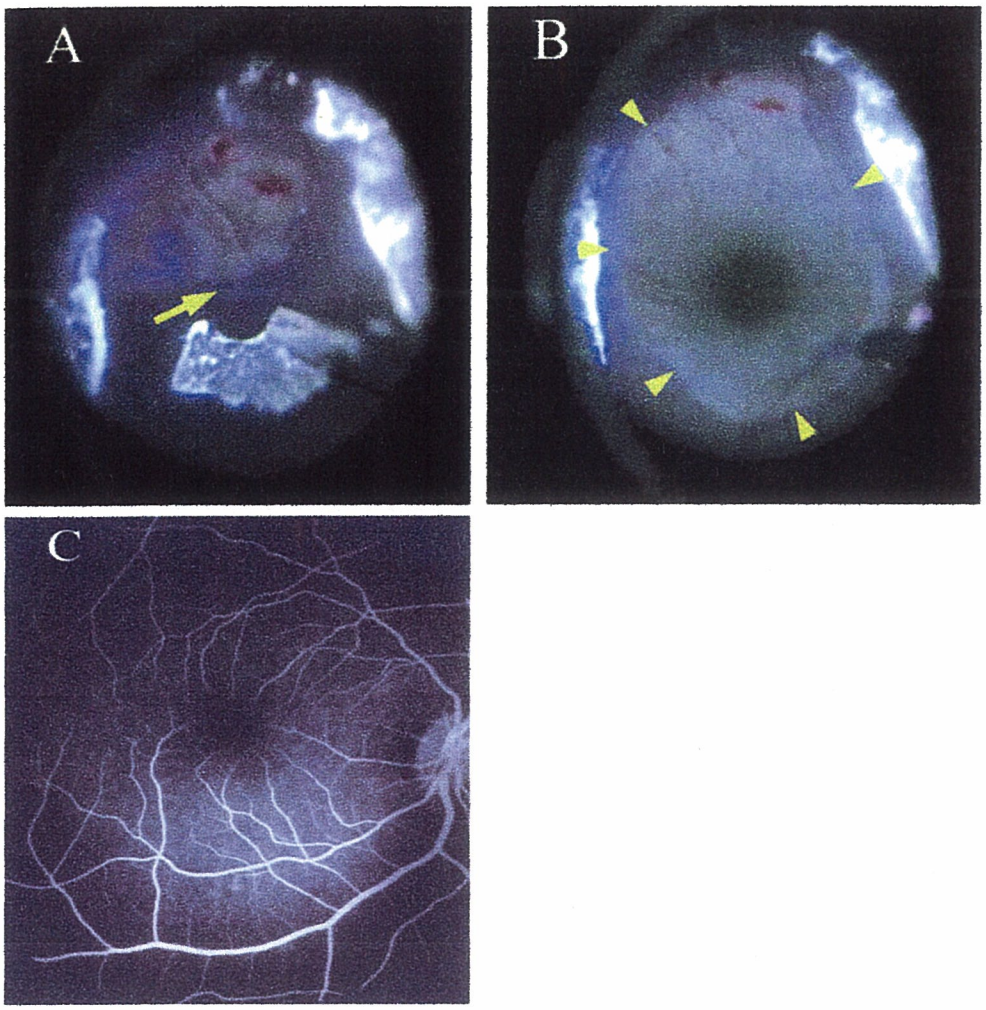

Fig. 5. Internal limiting membrane (ILM) staining by brilliant blue G (BBG) in primate eyes. The ILM was visualized by intravitreal injection of BBG. The arrow shows the ILM being removed from the retina with ILM forceps (**A**). The triamcinolone granules were trapped in the gel structure of the residual vitreous. After ILM removal, the difference in the retinal surface color between the area from which the ILM had been removed (arrowheads) and the surrounding area was clearly visible (**B**). No adverse effects of BBG on the retina were observed by fluorescein angiography (**C**; day 14).

mg/mL, $P = 0.508$; *t* test) and light-adapted *b* wave ERG (10 mg/mL, $P = 0.451$; and 1.0 mg/mL, $P = 0.550$; *t* test) demonstrated no remarkable reduction, with no statistically significant difference between the amplitudes (Fig. 4B; day 14). After 2 months, ERG recordings in the same dose groups (1.0 mg/mL and 10 mg/mL) were measured, and reduction of the amplitude of the dark-adapted *a* waves was found to recover in a manner similar to that in the control group.

BBG-Assisted ILM Peeling and Postoperative Examinations in Primate Eyes

The prepared BBG solution (0.5 mL) was injected gently into the vitreous cavity and washed out immediately with balanced salt solution. After irrigation of the vitreous cavity, the ILM was stained a light blue color. The edge and flap of the ILM were clearly visible during ILM peeling (Fig. 5A). The circular area underlying the ILM was clearly visible after ILM peeling (Fig. 5B).

Postoperatively, toxic effects of BBG, such as a corneal edema, severe retinal edema, and endophthalmitis, were not observed during slit-lamp microscopy and ophthalmoscopy at day 14. Fluorescein angiography also revealed that there was no apparent retinal damage by BBG on day 14 (Fig. 5C). Further ophthalmoscopic examinations showed no further changes in the retina during the 6-month follow-up period.

Discussion

The use of dyes such as ICG and TB has become a popular method to facilitate removal of the ILM and ERMs for treatment of various vitreoretinal diseases.[1–4] This technique has enabled surgeons to perform ILM and ERM peeling procedures with improved safety and ease.[5–7] However, adverse effects of these dyes on the retina have been widely reported in recent years.[8–21] Our previous studies have also shown the adverse effects of intravitreous ICG on the retina,[8] demonstrating that retinal damage can be caused by

phototoxicity[9] and the osmolarity[10] of ICG. TB, the other dye frequently used to assist in membrane peeling, is inferior to ICG in its ability to stain the ILM, and the surgical technique is also complicated by the need for fluid–gas exchange.[3,7] Furthermore, TB has also been recently reported to have a toxic effect on retinal cells.[14,20,21]

To select a suitable candidate for staining the ILM, we screened various dyes that were superior to ICG and TB in terms of their safety and membrane staining potential. Recently, we reported that BBG capsular staining contributed to better visualization during continuous curvilinear capsulorhexis in pig eyes.[22] BBG is a blue dye (color index 42655) with the formula $C_{47}H_{48}N_3O_7S_2Na$ (molecular weight, 854.0) that is also known as acid blue 90 and Coomassie BBG. BBG has been used for protein staining in biologic fields, because it binds nonspecifically to virtually all proteins. It is also used as a protein electrophoresis dye. The standard staining dose of the dye produced no apparent complications, with minimal changes in the corneal endothelium of rat eyes.[22] Furthermore, the staining ability of BBG solution is similar to that of ICG, thereby enabling a relatively simple surgical procedure to be performed.[22] The staining mechanism of BBG at the ILM still remains unknown. However, to the best of our knowledge, there have been no reports examining the clinical use of BBG in humans. The pharmacological function of the BBG still remains unconfirmed. However, although there are no reports on the medical use of this dye, there is a long history of biologic use in which no apparent toxicity has been reported. We therefore performed this study to investigate the possible use of BBG for safer membrane peeling in human eyes, because BBG is for experimental use only at present.

In our previous study, high doses (2.5 mg/mL and 25 mg/mL) of intravitreous ICG were found to cause morphologic damage in the rat retina when observed by light microscopy. In groups injected with low doses (0.025 and 0.25 mg/L), there was no apparent histologic damage, but the amplitude of the dark-adapted *b* waves decreased in a dose-dependent manner, producing a significant difference when compared with the controls. Similar findings were also observed in the rat eyes at 2 months after injection.[8] In the present study examining the safety of intravitreal BBG, the normal structure of the retina was preserved with all doses tested, both in groups enucleated on day 14 and at 2 months when examined using light microscopy. However, transmission electron microscopic observations revealed that the high-dose groups (10 mg/mL and 1 mg/mL) showed vacuolization in the ganglion cells and Müller cell processes in the nerve fiber layer. Because there have been several reports suggesting that damage of the retinal cells by ICG and TB is dependent on apoptotic cell death,[16–21] we investigated apoptotic cell death by TUNEL. Even in the group injected with the highest dose of BBG (10 mg/mL), however, no apparent apoptotic cell death was detected in the retina. In addition, we performed ERG to investigate retinal function. A slight reduction in the maximal amplitude of the dark-adapted *a* waves was observed in a dose-dependent manner on day 14 in the high-dose groups (1.0 mg/mL and 10 mg/mL); however, the difference between the high-dose and control groups was not significant. Because these changes had recovered to a level similar to that of the control group 2 months later, the influence of physical problems such as the high osmolarity of the high-dose BBG solution or technical problems of the ERG or operative stress were considered to cause the temporal dysfunction. From these results, we concluded that BBG has a better biocompatibility than ICG.

Because ILM peeling is impossible in rat eyes, we examined the ability of BBG to stain the ILM in primate eyes. After injecting 0.5 mg/mL BBG solution into primate eyes, the ILM was instantly stained light blue and was clearly visible. We were then able to easily remove the ILM with ILM forceps. Fluorescein angiography on day 14 also demonstrated that there was no apparent damage to the retina of primate eyes.

BBG also has a number of advantages over both ICG and TB in terms of handling. ICG is packaged as lyophilized powder and will not dissolve properly in intraocular irrigating solution alone. It therefore must be diluted in 0.5 mL of aqueous solvent before adding 4.5 mL of intraocular irrigating solution. BBG granules, by contrast, can be easily dissolved in intraocular irrigating solution alone and subsequently sterilized with a 0.22-μm syringe filter. The osmolarity and pH of the BBG solution are also very stable. Because BBG is not a fluorescent dye, the presence of light toxicity such as that found in ICG is highly unlikely. Furthermore, the staining process requires no additional techniques such as fluid–gas exchange that is necessary for TB application.

Although the surgical results of ILM or ERM peeling have been improved with the aid of ICG or TB staining,[1–7] surgeons should be aware of the possible adverse effects of these dyes when treating vitreoretinal diseases. The BBG concentration required for ILM staining in primates (0.5 mg/mL) is one tenth of that required for ICG (5 mg/mL). Further investigation is necessary before any clinical recommendation can be given. From our results, we conclude that BBG, which has low potential for toxicity, high staining ability,

and ease of handling, is a good candidate dye for ILM peeling.

Key words: brilliant blue G, vitrectomy, internal limiting membrane peeling, preclinical investigation, retinal function, retinal damage.

References

1. Burk SE, Da Mata AP, Snyder ME, et al. Indocyanine green-assisted peeling of the retinal internal limiting membrane. Ophthalmology 2000;107:2010–2014.
2. Kadonosono K, Itoh N, Uchio E, et al. Staining of internal limiting membrane in macular hole surgery. Arch Ophthalmol 2000;118:1116–1118.
3. Feron EJ, Veckeneer M, Parys-Van Ginderdeuren R, et al. Trypan blue staining of epiretinal membranes in proliferative vitreoretinopathy. Arch Ophthalmol 2002;120:141–144.
4. Perrier M, Sebag M. Trypan blue-assisted peeling of the internal limiting membrane during macular hole surgery. Am J Ophthalmol 2003;135:903–905.
5. Gandorfer A, Messmer EM, Ulbig MW, Kampik A. Indocyanine green selectively stains the internal limiting membrane. Am J Ophthalmol 2001;131:387–388.
6. Kusaka S, Hayashi N, Ohji M, et al. Indocyanine green facilitates removal of epiretinal and internal limiting membranes in myopic eyes with retinal detachment. Am J Ophthalmol 2001;131:388–390.
7. Haritoglou C, Eibl K, Schaumberger M, et al. Functional outcome after trypan blue-assisted vitrectomy for macular pucker: a prospective, randomized, comparative trial. Am J Ophthalmol 2004;138:1–5.
8. Enaida H, Sakamoto T, Hisatomi T, et al. Morphological and functional damage of the retina caused by intravitreous indocyanine green in rat eyes. Graefes Arch Clin Exp Ophthalmol 2002;240:209–213.
9. Sippy BD, Engelbrecht NE, Hubbard GB, et al. Indocyanine green effect on cultured human retinal pigment epithelial cells: implication for macular hole surgery. Am J Ophthalmol 2001;132:433–435.
10. Stalmans P, Van Aken EH, Veckeneer M, et al. Toxic effect of indocyanine green on retinal pigment epithelium related to osmotic effects of the solvent. Am J Ophthalmol 2002;134:282–285.
11. Gandorfer A, Haritoglou C, Gass CA, et al. Indocyanine green-assisted peeling of the internal limiting membrane may cause retinal damage. Am J Ophthalmol 2001;132:431–433.
12. Haritoglou C, Gandorfer A, Gass CA, et al. Indocyanine green-assisted peeling of the internal limiting membrane in macular hole surgery affects visual outcome: a clinicopathologic correlation. Am J Ophthalmol 2002;134:836–841.
13. Uemura A, Kanda S, Sakamoto Y, Kita H. Visual field defects after uneventful vitrectomy for epiretinal membrane with indocyanine green-assisted internal limiting membrane peeling. Am J Ophthalmol 2003;136:252–257.
14. Veckeneer M, van Overdam K, Monzer J, et al. Ocular toxicity study of trypan blue injected into the vitreous cavity of rabbit eyes. Graefes Arch Clin Exp Ophthalmol 2001;239:698–704.
15. Haritoglou C, Gandorfer A, Schaumberger M, et al. Trypan blue in macular pucker surgery: an evaluation of histology and functional outcome. Retina 2004;24:582–590.
16. Yam HF, Kwok AK, Chan KP, et al. Effect of indocyanine green and illumination on gene expression in human retinal pigment epithelial cells. Invest Ophthalmol Vis Sci 2003;44:370–377.
17. Kawaji T, Hirata A, Inomata Y, et al. Morphological damage in rabbit retina caused by subretinal injection of indocyanine green. Graefes Arch Clin Exp Ophthalmol 2004;242:158–164.
18. Rezai KA, Farrokh-Siar L, Ernest JT, van Seventer GA. Indocyanine green induces apoptosis in human retinal pigment epithelial cells. Am J Ophthalmol 2004;137:931–933.
19. Murata M, Shimizu S, Horiuchi S, Sato S. The effect of indocyanine green on cultured retinal glial cells. Retina 2005;25:75–80.
20. Rezai KA, Farrokh-Siar L, Gasyna EM, Ernest JT. Trypan blue induces apoptosis in human retinal pigment epithelial cells. Am J Ophthalmol 2004;138:492–495.
21. Kwok AK, Yeung CK, Lai TY, et al. Effects of trypan blue on cell viability and gene expression in human retinal pigment epithelial cells. Br J Ophthalmol 2004;88:1590–1594.
22. Hisatomi T, Enaida H, Matsumoto H, et al. The biocompatibility of brilliant blue G: preclinical study of brilliant blue G as an adjunct for capsular staining. Arch Ophthalmol (in press) .
23. Thresher RJ, Ehrenberg M, Machemer R. Gas-mediated vitreous compression: an experimental alternative to mechanized vitrectomy. Graefes Arch Clin Exp Ophthalmol 1984;221:192–198.
24. Irvine WD, Johnson MW, Hernandez E, Olsen KR. Retinal toxicity of human tissue plasminogen activator in vitrectomized rabbit eyes. Arch Ophthalmol 1991;109:718–722.
25. Araiz JJ, Refojo MF, Arroyo MH, et al. Antiproliferative effect of retinoic acid in intravitreous silicone oil in an animal model of proliferative vitreoretinopathy. Invest Ophthalmol Vis Sci 1993;34:522–530.
26. Bryan JS, Friedman SM, Mames RN, Margo CE. Experimental vitreous replacement with perfluorotri-n-propylamine. Arch Ophthalmol 1994;112:1098–1102.
27. Sakamoto T, Ueno H, Goto Y, et al. A vitrectomy improves the transfection efficiency of adenoviral vector-mediated gene transfer to Muller cells. Gene Ther 1998;5:1088–1097.
28. Hisatomi T, Sakamoto T, Murata T, et al. Relocalization of apoptosis-inducing factor in photoreceptor apoptosis induced by retinal detachment in vivo. Am J Pathol 2001;158:1271–1278.
29. Hisatomi T, Sakamoto T, Sonoda KH, et al. Clearance of apoptotic photoreceptors: elimination of apoptotic debris into the subretinal space and macrophage-mediated phagocytosis via phosphatidylserine receptor and integrin alphavbeta3. Am J Pathol 2003;162:1869–1879.
30. Goto Y, Yasuda T, Tobimatsu S, Kato M. 20-Hz flicker stimulus can isolate the cone function in rat retina. Ophthalmic Res 1998;30:368–373.
31. Goto Y, Tobimatsu S, Shigematsu J, et al. Properties of rat cone-mediated electroretinograms during light adaptation. Curr Eye Res 1999;19:248–253.
32. Sakamoto T, Miyazaki M, Hisatomi T, et al. Triamcinolone-assisted pars plana vitrectomy improves the surgical procedures and decreases the postoperative blood-ocular barrier breakdown. Graefes Arch Clin Exp Ophthalmol 2002;240:423–429.
33. Enaida H, Sakamoto T, Ueno A, et al. Submacular deposition of triamcinolone acetonide after triamcinolone-assisted vitrectomy. Am J Ophthalmol 2003;135:243–246.
34. Enaida H, Hata Y, Ueno A, et al. Possible benefits of triamcinolone-assisted pars plana vitrectomy for retinal diseases. Retina 2003;23:764–770.
35. Enaida H, Hata Y, Ueno A, et al. Visualization of the Cloquet canal during triamcinolone-assisted vitrectomy. Arch Ophthalmol 2004;122:1564–1565.

BRILLIANT BLUE G SELECTIVELY STAINS THE INTERNAL LIMITING MEMBRANE/BRILLIANT BLUE G–ASSISTED MEMBRANE PEELING

HIROSHI ENAIDA, MD,* TOSHIO HISATOMI, MD,* YASUAKI HATA, MD,* AKIFUMI UENO, MD,* YOSHINOBU GOTO, MD,† TOMOMI YAMADA, MS,‡ TOSHIAKI KUBOTA, MD,§ TATSURO ISHIBASHI, MD*

Purpose: To report the use of the dye brilliant blue G (BBG) for staining of the internal limiting membrane (ILM) during macular hole (MH) and epiretinal membrane (ERM) surgery.

Methods: This study was designed as an interventional, noncomparative, prospective, clinical case series. Twenty eyes from 20 consecutive patients with MH or ERM underwent BBG-assisted ILM and ERM removal. In MH cases, a posterior vitreous detachment was created, followed by the injection of 0.25 mg/mL BBG solution into the vitreous cavity and immediate washout of the BBG. This technique improved visualization of the ILM, enabling peeling and surgery to be performed successfully. However, in ERM cases, staining of the ERM could not be confirmed at this concentration. Finally, the ILM including the ERM was removed in all cases. Preoperative and postoperative ophthalmic examinations were performed.

Results: Postoperatively, 17 patients (85%) had visual acuity improved by at least 2 Snellen lines. No adverse effects were observed postoperatively during the observation period (mean follow-up ± SD, 7.3 ± 1.0 months).

Conclusions: BBG selectively stains the ILM. This technique can facilitate the management of MH and ERM surgery without any adverse effects, as was shown in this short-term study.

RETINA 26:631–636, 2006

Indocyanine green (ICG) staining and trypan blue (TB) staining have greatly facilitated internal limiting membrane (ILM) peeling in various vitreoretinal diseases.[1–6] However, numerous reports have emerged regarding retinal damage caused by ICG and TB in both experimental models and clinical use.[7–16] A dye with both satisfactory staining ability at low concentrations and minimal toxicity is required for effective membrane staining. We have screened various dyes focusing on their safety and ability to stain membranes during vitrectomy. From the results of our preclinical studies, we reported that brilliant blue G (BBG) membrane staining contributed to better visualization in continuous curvilinear capsulorhexis and ILM peeling in animal eyes.[17,18] The satisfactory staining dose of the dye provided no apparent complications, with minimal changes on the corneal endothelium and retinal cells of rat eyes.[17,18]

From the *Department of Ophthalmology, the †Department of Clinical Neurophysiology, and the ‡Department of Medical Information Science, Graduate School of Medical Sciences, Kyushu University, Fukuoka, Japan; and the §Department of Ophthalmology, University of Occupational and Environmental Health, Kitakyushu, Japan.

Supported in part by Grant-in-Aids 16791052 and 14571676 for Scientific Research from the Japanese Ministry of Education, Science, Sports and Culture.

Reprint requests: Tatsuro Ishibashi, MD, Department of Ophthalmology, Graduate school of Medical Sciences, Kyushu University, 3-1-1 Maidashi, Higashi-ku, Fukuoka, 812-8582, Japan; e-mail: ishi@eye.med.kyushu-u.ac.jp

Table 1. Clinical Parameters for MH Patients

Case No./ Age (y)/ Sex	MH Stage	Preop BCVA	Postop BCVA	ILM Peeling	Postop Retinal Status	Lens Status Preop/Postop	Postop IOP Elevation	Complication	Follow-up (mo)
1/58/F	3	20/63	20/20	+	MH closed	Phakic/IOL	–	None	9
2/77/M	4	20/200	20/200	+	MH closed	Phakic/IOL	–	None	8
3/57/F	3	20/50	20/32	+	MH closed	Phakic/IOL	–	None	7
4/62/F	2	20/100	20/25	+	MH closed	Phakic/IOL	–	None	7
5/68/M	3	20/100	20/40	+	MH closed	Phakic/IOL	–	Peripheral retinal break	7
6/79/M	3	20/80	20/50	+	MH closed	IOL/IOL	–	Peripheral retinal break	7
7/78/M	3	20/125	20/25	+	MH closed	Phakic/IOL	+	None	7
8/63/F	3	20/50	20/20	+	MH closed	Phakic/IOL	–	None	7
9/64/F	2	20/63	20/25	+	MH closed	Phakic/IOL	–	None	7
10/73/M	4	20/200	20/50	+	MH closed	Phakic/IOL	–	None	6

MH, macular hole; preop, preoperation; BCVA, best-corrected visual acuity; postop, postoperation; ILM, internal limiting membrane; IOP, intraocular pressure; +, present; IOL, intraocular lens; -, absent.

In this study, we investigated the staining pattern of the membranes and clinical outcome using BBG in macular hole (MH) and epiretinal membrane (ERM) cases. This study was designed as an interventional, noncomparative, prospective, clinical case series.

Methods

Twenty eyes from 20 consecutive patients presenting with MH (10 eyes from 10 patients; 5 men and 5 women) or ERM (10 eyes from 10 patients, 5 men and 5 women) underwent vitrectomy with removal of the membranes using BBG staining solution between August and November 2004. Patients with ocular diseases such as glaucoma, diabetic retinopathy, uveitis, and corneal disorder were excluded. The mean age ± SD of the patients was 67 ± 11.9 years (range, 33–85 years). The mean follow-up ± SD was 7.3 ± 1.0 months. Patient characteristics are summarized in Tables 1 and 2. Preoperative and postoperative ophthalmic examinations included slit-lamp microscopy, ophthalmoscopy, and determinations of best-corrected visual acuity (BCVA) and intraocular pressure. MH closure and measurement of foveal thickness (ERM cases) were determined by optical coherence tomography (OCT3; Humphrey Instruments, San Leandro, CA). The mean foveal thickness was calculated from a total of four scans.

Excised specimens from four eyes (two eyes of MH patients and two eyes of ERM patients) were submitted for transmission electron microscopy to verify the presence of ILM. The specimens were postfixed in veronal acetate buffer osmium tetroxide (2%), dehydrated in ethanol and water, and embedded in Epon (Epon 812 Resin, CHIYODA JYUNYAKU INC., Tokyo, Japan). Ultrathin sections were cut from blocks and mounted on copper grids. The specimens were observed with a JEM 100CX electron microscope (JEOL, Tokyo, Japan).

Table 2. Clinical Parameters for ERM Patients

Case No./ Age (y)/ Sex	ERM Status	Preop BCVA	Postop BCVA	ILM Peeling	Retinal Thickness Preop/Postop (μm)	Lens Status Preop/Postop	Postop IOP Elevation	Complication	Follow-up (mo)
1/33/M	Secondary	20/63	20/32	+	759/232	IOL/IOL	–	None	9
2/85/M	Primary	20/50	20/32	+	441/248	Phakic/IOL	–	None	9
3/72/F	Primary	20/63	20/50	+	423/354	Phakic/IOL	–	None	8
4/85/M	Primary	20/63	20/32	+	478/266	Phakic/IOL	–	Vitreous bleeding	8
6/66/F	Primary	20/40	20/12.5	+	501/240	Phakic/IOL	–	None	7
6/72/M	Primary	20/40	20/16	+	417/190	Phakic/IOL	–	None	7
7/63/F	Primary	20/63	20/25	+	429/232	Phakic/IOL	–	None	7
8/69/F	Primary	20/100	20/100	+	556/382	Phakic/IOL	–	None	6
9/56/M	Pseudo MH	20/40	20/20	+	228/146	Phakic/IOL	–	None	6
10/60/F	Primary	20/40	20/25	+	315/204	IOL/IOL	–	None	6

ERM, epiretinal membrane; preop, preoperation; BCVA, best-corrected visual acuity; postop, postoperation; ILM, internal limiting membrane; IOP, intraocular pressure; +, present; IOL, intraocular lens; -, absent; MH, macular hole.

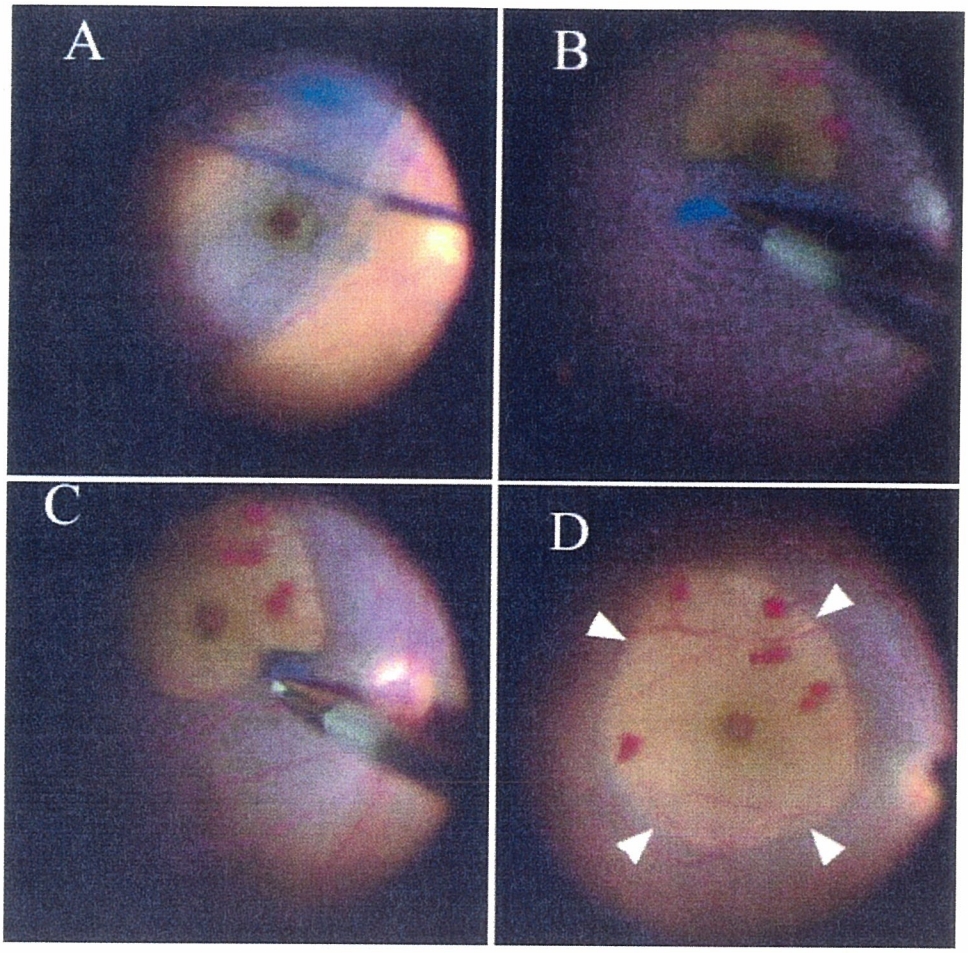

Fig. 1. Brilliant blue G (BBG)–assisted internal limiting membrane (ILM) peeling for macular hole (MH). The prepared BBG solution (0.25 mg/mL) was injected gently into the vitreous cavity (**A**) and washed out immediately with balanced salt solution. In MH cases, the ILM was stained a light blue color instantly. The edge and flap of the ILM were clearly visible during the ILM peeling (**B** and **C**). After ILM removal, the difference of the retinal surface between the area from which the ILM had been removed and the surrounding area was clearly visible (arrowheads; **D**).

This study was carried out with approval from the institutional review board and performed in accordance with the ethical standards of the 1989 Declaration of Helsinki. The possible advantages and risks of the present treatment were explained to all patients before surgery, and written informed consent was obtained from the patients.

Surgical Technique

Standard phacoemulsification was performed when needed. Surgery consisted of three-port pars plana vitrectomy with induction of a posterior vitreous detachment by suction with a vitrectomy cutter using triamcinolone acetonide injection (Kenakolt-A; Bristol Pharmaceuticals KK, Tokyo, Japan) as required.[19–21] BBG (brilliant blue G 250; Sigma–Aldrich, St. Louis, MO) was dissolved in intraocular irrigating solution (OPEGUARD-MA; Senjyu Pharmaceutical, Osaka, Japan). The solution was then sterilized through a 0.22-μm syringe filter.[22,23] The final concentration of BBG was 0.25 mg/mL (289 mosm; pH = 7.44). The prepared BBG solution (0.5 mL) was then injected gently into the vitreous cavity (Fig. 1A) and washed out immediately with balanced salt solution (BSS plus; Santen, Osaka, Japan). In MH cases, the ILM was stained a bright blue color instantly. Removal of the ILM was performed using ILM forceps (Fig. 1, B and C). After ILM removal, the difference in the retinal surface color between the area from which the ILM had been removed and the surrounding area was clearly visible (Fig. 1D). In ERM cases, however, staining of the ERM could not be confirmed at this concentration (Fig. 2A). After ERM peeling (Fig. 2B), BBG solution was injected again, followed by immediate irrigation of the vitreous cavity. The ILM of the area where the ERM had been removed was well stained with BBG (Fig. 2C). However, the area where residual ERM and posterior vitreous remained was not stained. The well stained ILM could be easily removed with unstained residual ERM and posterior vitreous (Fig. 2D).

Finally, intraocular lenses were inserted in all cases.

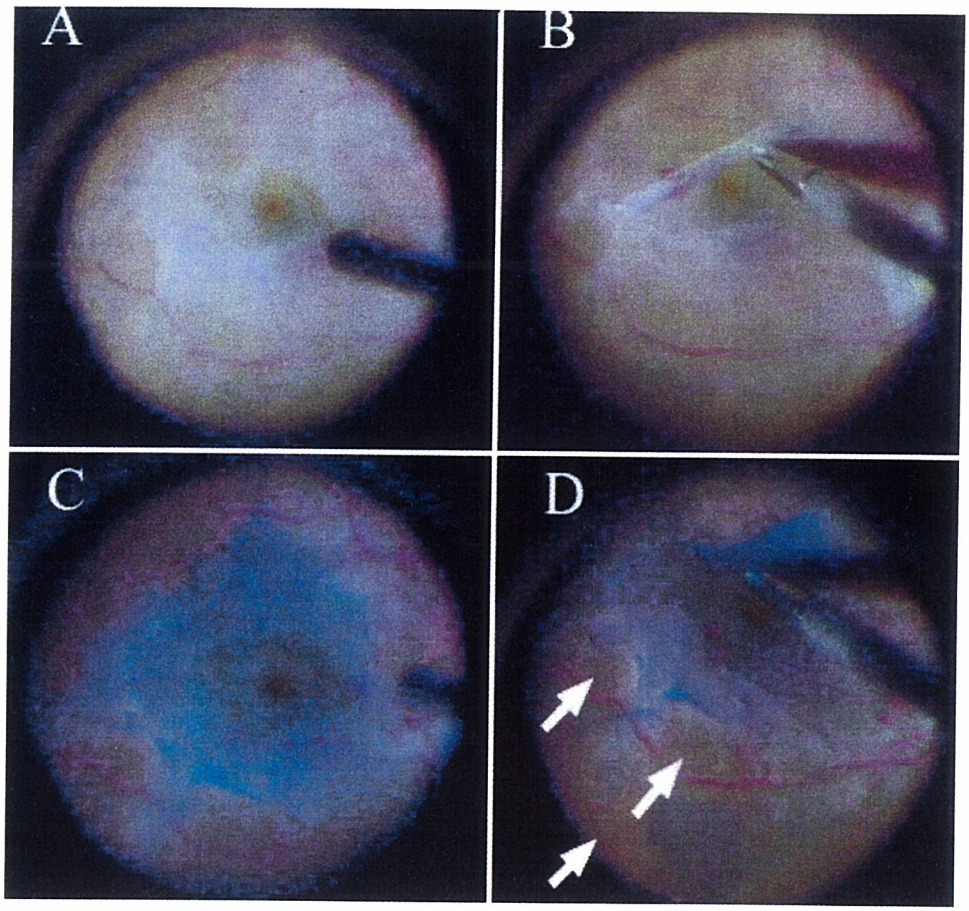

Fig. 2. Brilliant blue G (BBG)–assisted membrane peeling for epiretinal membrane (ERM). Staining of the ERM could not be confirmed at this concentration (**A**). After peeling of the ERM (**B**), BBG solution was injected again, and the vitreous cavity was irrigated immediately. The internal limiting membrane (ILM) of the area from which the ERM had been removed was well stained (**C**). The arrows show that the area where residual ERM and the posterior vitreous remained was not stained. The well stained ILM was easily removed (**D**).

In MH cases, fluid–gas exchange was performed and was replaced with 15% sulfur hexafluoride gas. Patients were advised to maintain a face down posture for 1 week.

Results

The ILM including the ERM was removed from all 20 eyes successfully during surgery. Transmission electron microscopy confirmed the presence of the ILM in all processed specimens (n = 4) (Fig. 3). Postoperatively, any acute toxicity induced by BBG injection, such as corneal edema, severe retinal edema, and severe intraocular inflammation such as endophthalmitis, was not observed by slit-lamp microscopy and ophthalmoscopy by day 14.

All MHs were completely closed anatomically as shown by both ophthalmoscopy and optical coherence tomography. The preoperative median BCVA was 20/100 (range, 20/200 to 20/50). The postoperative median BCVA was 20/32 (range, 20/200 to 20/20). Visual acuity improved in 9 eyes (90%) by ≥2 Snellen lines and was unchanged in 1 eye. In two cases, complications included iatrogenic peripheral retinal breaks, which were treated by endolaser photocoagulation intraoperatively. In only one MH case was there an elevation of IOP (26 mmHg) after 6 months, and this was treated with latanoprost (Xalatan®, Pfizer Japan Inc., Tokyo, Japan) (Table 1).

In ERM cases, the mean foveal thickness of retina ± SD measured by optical coherence tomography decreased from 454.7 ± 141.3 μm (preoperative) to

Fig. 3. Transmission electron micrographs of the removed internal limiting membrane (ILM). The removed ILM shows an irregular surface on the retinal side (R), which is associated with fragments of Müller cells (arrowheads). The vitreous side showed a smooth surface (V). This examination confirmed the presence of the ILM in all processed specimens from four eyes (original magnification, ×2,600).